RevMexAA (Serie de Conferencias), **27**, 57–79 (2007)

LAST MOMENTS IN THE LIFE OF A COMPACT BINARY SYSTEM: GRAVITATIONAL WAVES, GAMMA-RAY BURSTS AND MAGNETAR FORMATION

S. Rosswog[1]

Received 2006 March 20; accepted 2006 December 20

RESUMEN

Las primeras detecciones de contrapartes en emisión de rayos X y óptico para destellos de rayos gama (DRGs) cortos han confirmado la sospecha de que la fuente es distinta a la que opera en destellos largos. En particular, su detección en galaxias con poca o nula formación estelar argumentan en favor de una población estelar evolucionada. Los candidatos más fuertes involucran la fusión de una binaria con dos estrellas de neutrones o una estrella de neutrones y un agujero negro. Dado que la identificación del objeto central sólo podrá darse basado en propiedades integrales, hacemos aquí una revisión de las señales observables que podrían esperarse de estos sistemas. Discutimos la emisión de ondas gravitacionales, la estructura de discos de acreción enfriados por neutrinos, así como los mecanismos capaces de producir el destello en sí. También abordamos la idea, más especulativa, de que en algunos casos la fusión de dos estrellas de neutrones puede dar lugar a un magnetar, u objeto similar. Finalmente, discutimos algunas posibilidades para explicar la emisión tardía en ráfagas de rayos X observada en algunos eventos.

ABSTRACT

The first detections of afterglows from *short* gamma-ray bursts (GRBs) have confirmed the previous suspicion that they are triggered by a different central engine than long bursts. In particular, the recent detections of short GRBs in galaxies without star formation lends support to the idea that an old stellar population is involved. Most prominent are mergers of either double neutron stars or of a neutron star with a stellar-mass black hole companion. Since the final identification of the central engine will only come from an integral view of several properties, we review the observable signatures that can be expected from both double neutron stars and neutron star black hole systems. We discuss the gravitational wave emission, the structure of the neutrino-cooled accretion disks, the resulting neutrino signal and possible mechanisms to launch a GRB. In addition, we address the speculative idea that in some cases a magnetar-like object may be the final outcome of a double neutron star merger. We also discuss possibilities to explain the late-time X-ray activity that has been observed in several bursts.

Key Words: **GAMMA-RAYS: BURSTS — GRAVITATIONAL WAVES — ISM: JETS AND OUTFLOWS — PULSARS: GENERAL — STARS: NEUTRON**

1. INTRODUCTION

Gamma-ray bursts (GRBs) are subdivided on grounds of both their durations and spectra into short-hard and long-soft bursts (Kouveliotou et al. 1993). While a lot has been learned from the detection of long GRB afterglows since 1997 (Costa et al. 1997; van Paradijs et al. 1997; Frail et al. 1997; Bloom et al. 1999; Stanek et al. 2003; Hjorth et al. 2003), for example that long GRBs are related to death of massive stars in star-forming regions, the afterglows of short GRBs remained elusive until the early summer of 2005. The recent detections of afterglows from short GRBs point to a central engine that is related to an old stellar population. In particular, it has been argued (Bloom et al. 2006; Berger et al. 2005; Barthelmy et al. 2005; Villasenor et al. 2005) that the observations are consistent with being the result of compact binary mergers: they occur systematically at lower redshifts[2] than their long-duration cousins (e.g. Fox et al. 2005), both in galaxies with (Hjorth et al. 2005) and without

[1]School of Engineering and Science, International University Bremen, Germany. Jacobs University Bremen as of spring 2007.

[2]It has recently been suggested (Berger et al. 2006b) that at least 1/4 of the short bursts could lie at redshifts $z > 0.7$ and would therefore imply substantially larger isotropised energies than was inferred for the first set of detected short GRBs with afterglows.

star formation (Berger et al. 2005; Barthelmy et al. 2005) and they are not accompanied by a detectable supernova explosion (Bloom et al. 2006; Fox et al. 2005; Hjorth et al. 2005).

There are, however, puzzling observations of late-time flaring activity in several short bursts (Berger et al. 2006a). For example, GRB050724 showed long-lasting ($\sim$ 100s) X-ray flaring activity after a delay of $\sim$ 30 s. These long-lasting flares motivated MacFadyen, Ramirez-Ruiz, & Zhang (2005) to suggest an accretion-induced collapse of a neutron star in a low-mass X-ray binary as an alternative central engine. This central engine would produce the flaring by interaction of the GRB outflow with the non-compact companion star.

As the final identification of the central engine will probably only come from an integral view of various features from a large sample of events, we will give an overview over the properties and signatures that can be expected from compact binary mergers. They will include gravitational waves, the structure of the forming accretion disk, the neutrino emission and the burst itself. Moreover, we will discuss possibilities to produce the observed late-time flaring activity.

The discussion is mostly based on own simulations, some of which have been reported previously (Rosswog & Davies 2002a; Rosswog & Ramirez-Ruiz 2002b, 2003b; Rosswog & Liebendörfer 2003a; Rosswog et al. 2003a, 2004; Rosswog 2005) and several new simulations that are introduced here, see Table 1. The physics included in our models and the numerical techniques that we use have been described in a series of papers (Rosswog & Davies 2002a; Rosswog & Liebendörfer 2003a; Rosswog et al. 2003c, 2004).

The new neutron star merger calculations have been produced with a new Smoothed Particle Hydrodynamics (SPH) code that benefits from a slew of numerical improvements. It incorporates

- an artificial viscosity oriented at Riemann solvers, see Chow & Monaghan (1997),
- a consistent accounting of the effects of the so-called "grad-h"-terms, see Springel & Hernquist (2002), Monaghan (2002) and Price (2004),
- a consistent implementation of adaptive gravitational softening lengths, see Price & Monaghan (2007),
- the option to evolve magnetic fields together with the fluid, either via so-called Euler potentials (Stern 1970) or via a SPH discretisation of the MHD-equations (Price & Monaghan 2005).

First results obtained with this code have been published (Price & Rosswog 2006), a detailed code documentation can be found in Rosswog & Price (2006).

2. GRAVITATIONAL WAVES AS PROBES OF THE COALESCENCE DYNAMICS

Gravitational waves can serve as a direct probe of the merger dynamics and, if detected coincident with a short GRB, they would provide the ultimate proof of the compact binary nature of the central engine. The dynamics of the merger process is sensitive to the mass ratio of the involved components, therefore, the signal from the merger of a double neutron star system (DNS) with a mass ratio close to unity can be very different from a neutron star black hole (NSBH), where the black hole can, in principle, be much more massive than the neutron star.

In the last minutes before the coalescence the gravitational wave signal will slowly sweep through the frequency range that is accessible to ground-based gravitational wave-detectors such as GEO600 (Grote et al. 2005), LIGO (Abramovici et al. 1992), TAMA (Ando et al. 2004) or VIRGO (Spallici et al. 2005; Freise 2005). The detection of a gravitational wave signal coincident with a short GRB would allow to determine the distance to the source, the luminosity and the beaming angle (Kobayashi & Mészáros2003).

The coalescence of a double neutron star system can be divided into three phases: the secular inspiral due to gravitational wave emission, the actual merger and, finally, the "ring-down" phase, in which the death-struggle of the freshly formed supermassive neutron star will take place. After this phase the remnant will have settled into its final state, probably a black hole (an alternative is discussed in Section 6).

During the inspiral, the gravitational wave forms can be accurately described via post-Newtonian expansions for point masses. To date, post-Newtonian formalisms exist up to 3.5PN order, see Blanchet (2006) for a recent review, and lowest order spin-spin and spin-orbit couplings can be accounted for (e.g. Will 2005). In the inspiral phase, both the frequency and the amplitude of the waves will increase, the system is said to "chirp". The orbit decays secularly until the last stable orbit is reached, where the binary enters a "plunging phase". In this phase the stars fall nearly radially towards each other and merge within about one orbital period. This dynamical instability (Chandrasekhar 1975; Tassoul 1975) is

TABLE 1

NEW RUNS: DNS STANDS FOR DOUBLE NEUTRON STAR SYSTEMS, NSBH FOR NEUTRON STAR BLACK HOLE SYSTEMS. M_1 AND M_2 ARE THE COMPONENT MASSES, Q IS THE MASS RATIO, A_0 IS THE INITIAL SEPARATION, N STANDS FOR NEWTONIAN, PW FOR THE Paczyński-WIITA PSEUDO-POTENTIAL, $R_{\rm ABS}$ IS THE RADIUS OF THE ABSORBING BOUNDARY, IN UNITS OF $GM_{\rm BH}/C^2$, THE NEXT COLUMN GIVES THE SPH PARTICLE NUMBER

run	type	M_1	M_2	q	a_0 [km]	grav.	$R_{\rm abs}$	SPH part.
DA	DNS	1.4	1.4	1	48	N	-	$2 \cdot 10^6$
DB	DNS	1.1	1.6	0.6875	48	N	-	$5 \cdot 10^5$
NA	NSBH	1.4	3.0	0.4667	60	N	6	$6 \cdot 10^5$
NB	NSBH	1.4	4.0	0.35	72	N	6	$2 \cdot 10^5$
NC	NSBH	1.4	7.0	0.2	90	N	6	$2 \cdot 10^5$
ND	NSBH	1.4	10.0	0.14	112.5	PW	3	$2 \cdot 10^5$

the result a steepening of the gravitational potential due to both purely Newtonian tidal (Lai et al. 1993) and general relativistic effects, for a recent review on relativistic binaries see Baumgarte & Shapiro (2003). For the last two phases, the merger and ringdown, three-dimensional hydrodynamic simulations are required to predict the gravitational wave signal.

Double neutron star merger wave forms has been predicted by several groups. The calculations started with Newtonian calculations (e.g. Oohara & Nakamura 1989; Rasio & Shapiro 1994; Ruffert et al. 1997; Ruffert & Janka 2001). Post-Newtonian approaches (Ayal et al. 2001; Faber & Rasio 2000) turned out not to be particularly successful due to the importance of higher order PN-corrections. In the conformal flatness approach (Isenberg 1978; Wilson et al. 1996) it is assumed that the dynamical degrees of freedom of the gravitational fields, i.e. gravitational waves, can be neglected and that the spatial part of the metric is (up to a conformal factor) flat and remains so during the further evolution. This approximation has been used in several compact binary simulations (e.g. Wilson et al. 1996; Oechslin et al. 2002, 2004; Faber et al. 2004; Oechslin,Janka, & Marek 2006) and it could be shown (Cook, Shapiro, & Teukolsky 1996) to be provide reasonable accuracy in several cases. Finally, fully relativistic simulations have been performed by Shibata and collaborators (Shibata 1999; Shibata & Uryu 2002; Shibata et al. 2005). For a recent review on numerical relativity and compact binaries we refer to Baumgarte & Shapiro (2003).

The simulation of neutron star black hole binaries has been somewhat lagging behind the DNS status. Again, first simulations were Newtonian (e.g. Lee 1999a,b; Janka 1999; Lee 2000, 2001; Rosswog et al. 2004), slightly later followed simulations that used a Paczyński-Wiita (1980) pseudo-potential (Lee & Kluzńiak 1999a; Rosswog 2005; Setiawan, Ruffert, & Janka 2004, 2006). Very recently, progress has been made with relativistic approaches. For example, Taniguchi et al. (2005) were able to construct general relativistic quasi-equilibrium sequences for black holes that are much more massive than the neutron star. Faber et al. (2006) used an exact metric together with a conformal flatness approach in which the black hole position was artifically kept fixed in space. Löffler, Rezzolla, & Ansorg (2006) were able to treat binary components of comparable mass, but their approach was restricted to a head-on collision. Recently, Shibata & Uryu (2006) reported on first results of neutron star black hole binaries in full general relativity.

Here, we will report mainly on our own, either Newtonian or pseudo-Newtonian results. These calculations focused on the microphysics rather than the strong-field gravity aspect, therefore, the results concerning gravitational waves should be taken with a grain of salt. Details about the calculation of the wave forms can be found in Rosswog et al. (2004), we will mention in the appropriate places in which direction fully relativistic calculations are expected to change the results.

2.1. *Double neutron stars*

For many years, neutron star masses, at least those in double neutron star systems, were thought to be tightly clustered around a mass of m=1.35 $M_\odot$ (Thorsett & Chakrabarty 1999). Re-

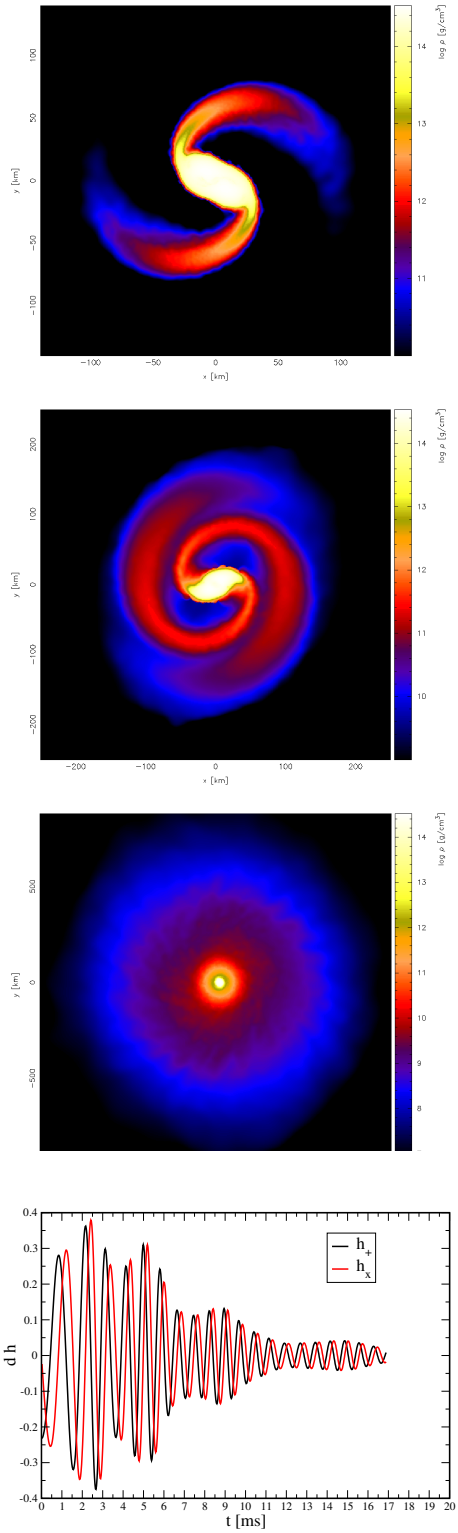

Fig. 1. Merger of a double neutron star system with 1.4 $M_\odot$ each (snapshots at 4.41, 5.54 and 15.0 ms). The lowest panel shows the gravitational wave amplitudes times the distance to the source, d (in units of 1.5 km).

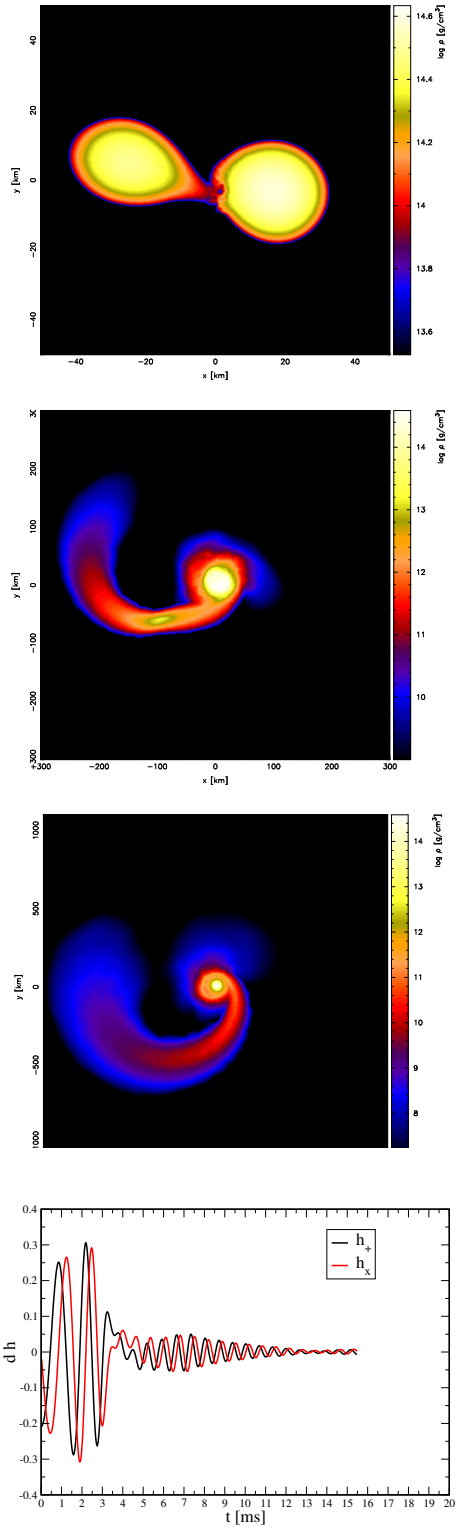

Fig. 2. DNS merger with 1.1 and 1.6 $M_\odot$ (at 1.51, 6.17 and 15.0 ms). The lowest panel shows the gravitational wave amplitudes times the distance to the source, d (in units of 1.5 km), as a function of time.

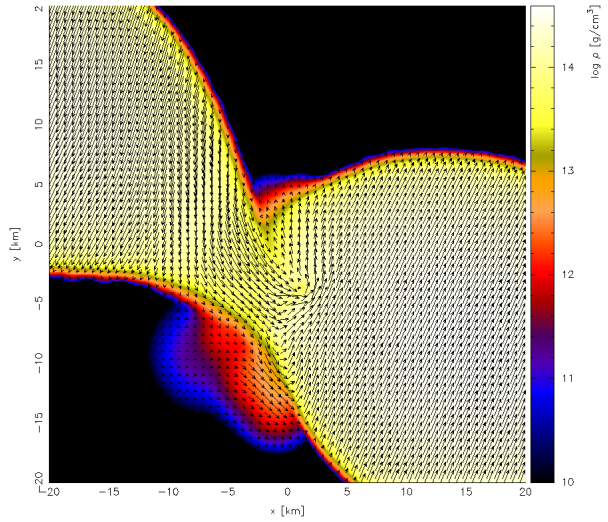

Fig. 3. Merger of 1.1 and 1.6 $M_\odot$ system (t=1.39 ms): Impact of accretion stream onto surface of accreting neutron star. Color-coded is density in the orbital plane, the arrows indicate velocities.

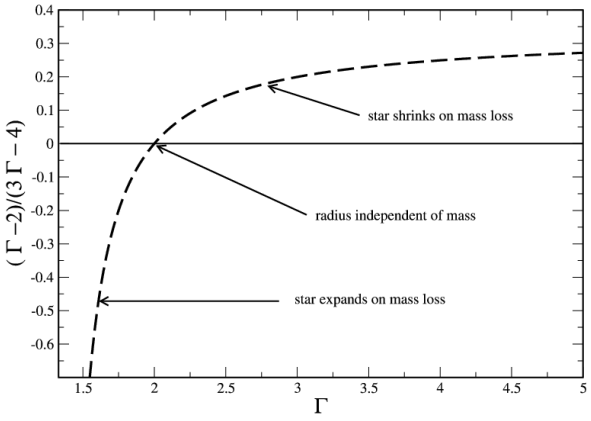

Fig. 4. Exponent of the mass-radius relationship for a polytropic star.

cent data, see e.g. Stairs (2004), show considerable deviations from this value for several of the known binary systems. The recently discovered double neutron star system PSR J1756-2251 (Faulkner et al. 2005), for example, has a mass ratio of q=0.84 ($m_1 = 1.40$ and $m_2 = 1.18$ $M_\odot$) and the double neutron star J1518+4904 even has $q = 0.67$ ($m_1 = 1.56$ and $m_2 = 1.05$ $M_\odot$), but still relatively large errors (see Stairs 2004).

For our new DNS simulations, we take masses of twice 1.4 $M_\odot$ as the typical case, but we also consider the more extreme case with a 1.1 and a 1.6 $M_\odot$ neutron star. The dynamical evolution during the last moments of a binary system with twice 1.4 $M_\odot$ is shown in Figure 1. The neutron stars have no initial spin, their initial separation is just outside the plunging regime for our equation of state at 48 km and each star is modelled with slightly more than a million SPH particles (run DA in Table 1). Once the plunging sets in, the stars merge within about one orbital revolution. Excess angular momentum is shed into symmetric spiral arms that subsequently spread into an extended accretion disk, see Section 3, around a super-massive, neutron star-like object. The evolution of the 1.1 and 1.6 $M_\odot$ system (run DB in Table 1), similar to J1518+4904, is shown in Figure 2. In this case the lighter star starts to transfer mass towards and then completely engulfs the more massive component. The mass transfer leads to a complete tidal disruption of the 1.1 $M_\odot$ star, parts of which form a tidal tail, see panel three of Figure 2. For the chosen system parameters, the circularization radius of the accreted material is smaller than the accretor radius, therefore, like in an Algol system, the accretion stream directly impacts on the accretor crust, see panel one in Figure 2 and Figure 3. For less extreme mass ratios the accreted material slides more smoothly around the surface of the heavier companion, otherwise the evolution is similar.

In the last panels of Figures 1 and 2 we show the retarded gravitational wave amplitudes, h_+ and $h_\times$, as seen along the binary axis by a distant observer at distance d. In both cases one sees the last stages of the "chirp"-signal up to about 2.5 ms, when the stars come into contact. For the chosen initial separation of the 2×1.4 $M_\odot$ case the peak frequency of $\approx$ 1 KHz is reached 2.5 ms after the simulation start. If $h_{\rm min}$ labels the minimum detectable amplitude, such a system would be visible out to a distance $d = 18{\rm Mpc}(10^{-21}/h_{\rm min})$. During the chirp phase up to about 2.5 ms the signal is the result of the binary orbital motion, after that, up to about 6 ms it is determined by the elongated central object and the spiral arms. The central object does not become rotationally symmetric by the end of the simulation and, therefore, keeps emitting quasi-periodic gravitational waves at about a tenth of the amplitude. This is behaviour is expected for a stiff equation of state (EOS) such as the Shen et al. (1998) EOS that we use. It had been noted very early on (Rasio & Shapiro 1994) that this post-merger gravitational wave signal is a way to constrain the equation of state.

For the 1.1-1.6 $M_\odot$ system the peak frequency is slightly lower, $\nu_{\rm peak} \approx 780$ Hz, the same statement is true for the peak amplitude.

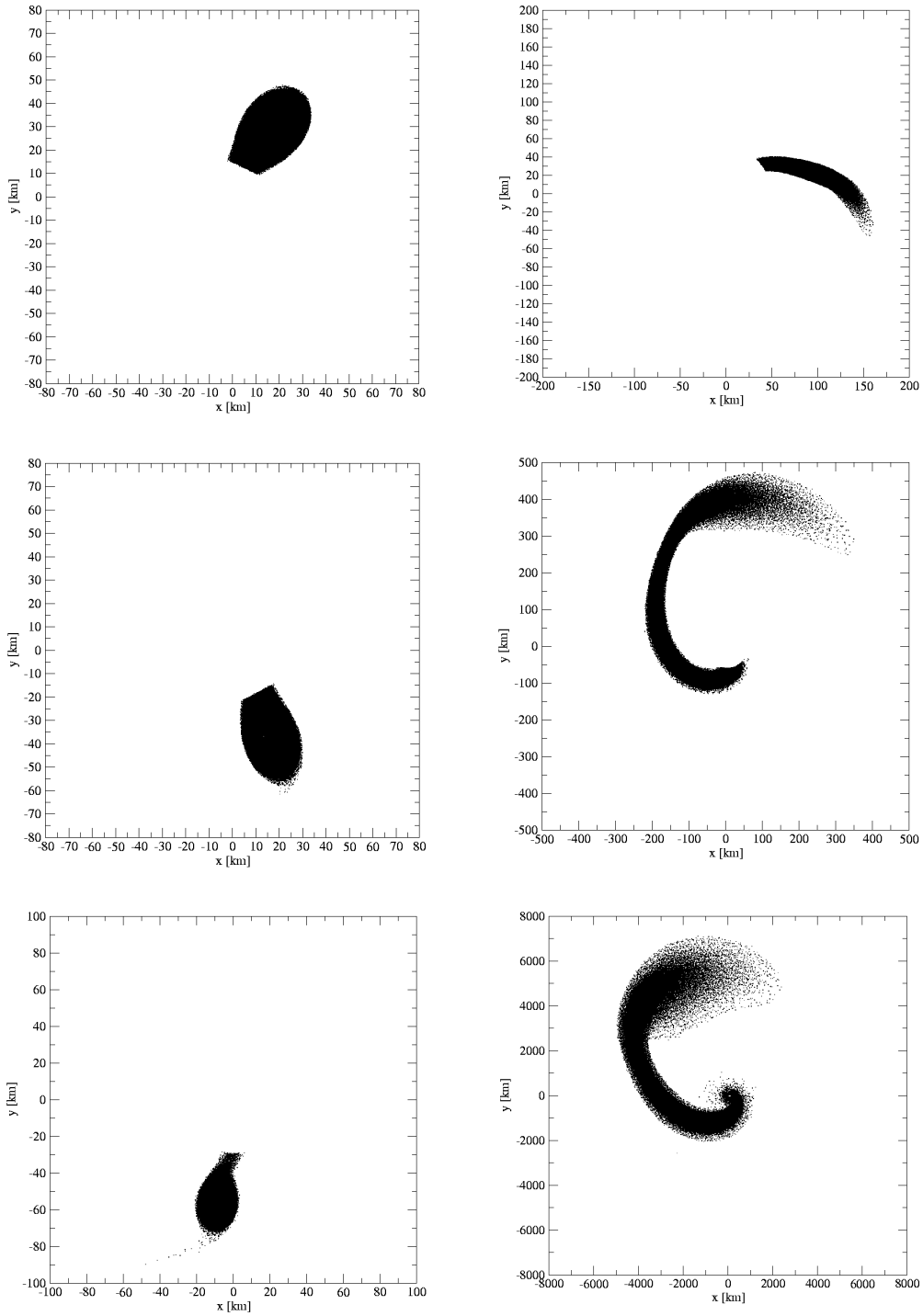

Fig. 5. Dynamical evolution of a neutron star black hole system. Left column: example of a system that undergoes episodic mass transfer (M_{ns}=1.4 $M_\odot$, M_{bh}=3 $M_\odot$). A mini-neutron star keeps orbiting the hole, thereby transfers mass directly into the hole and sheds mass which subsequently spreads into a dilute disk surrounding the orbiting binary system. It is only after 47 orbital revolutions ($t \approx 220$ ms) that the mini-neutron star is finally disrupted, see panel 4, and its remains form an accretion disk of ≈ 0.05 $M_\odot$, see Figure 11. This episodic mass transfer is imprinted on the gravitational wave signal, see Figure 9. Right column: binary in which the neutron star is directly disrupted (M_{ns}=1.4 $M_\odot$, M_{bh}=14 $M_\odot$). The figures in each column refer to 3, 5 and 37 ms, respectively, after the onset of mass transfer.

This basic picture of the dynamical evolution carries over to general relativistic calculations. The stronger gravity, however, produces neutron stars of higher compactness and a more compact remnant. Apart from the most obvious consequence, the possible gravitational collapse to a black hole, a general relativistic merger yields higher peak frequencies and gravitational wave amplitudes and therefore ensures detectability out to larger distances. For more details we refer to the recent calculations of Shibata et al. (2005).

2.2. *Neutron star black hole*

The accretion and merger dynamics of neutron star black hole systems is, mainly due to the larger possible mass ratios, substantially more complicated. It is a result of the interplay between gravitational wave emission, mass transfer and the nuclear EOS (Rosswog et al. 2004). Gravitational wave emission will drive the binary towards coalescence, the mass transfer from the lighter neutron star to the heavier black hole has the opposite tendency. The influence of the EOS is twofold. On the one hand it determines the radius of the star, $R_{\rm ns}$, and therefore the tidal radius, at which the neutron star will be disrupted. A simple estimate for this radius is given by

$$R_{\rm tid} = \left(\frac{M_{\rm bh}}{M_{\rm ns}}\right)^{1/3} R_{\rm ns}. \qquad (1)$$

On the other hand the EOS is responsible for the way the star reacts to mass loss, i.e. whether it expands or contracts. For a polytropic star the mass-radius relationship is $R \propto M^{\frac{\Gamma-2}{3\Gamma-4}}$, where Γ is the polytropic exponent of the EOS (e.g. Kippenhahn & Weigert 1990). The exponent of the mass-radius relation of a polytropic star, $(\Gamma-2)/(3\Gamma-4)$, is plotted in Figure 4. For $\Gamma < 2$ the star expands on mass loss and for $\Gamma > 2$ it shrinks on mass loss. For a realistic EOS, however, the situation is complicated by the fact that Γ changes with density. For the EOS we use (Shen et al. 1998), the neutron star will shrink on mass loss for masses above 0.4 $M_\odot$ and expand otherwise.

To build up an accretion disk a large ratio of tidal radius to innermost stable circular orbit, $R_{\rm isco}$,

$$\frac{R_{\rm tid}}{R_{\rm isco}} = \frac{c^2}{6G}\frac{R_{\rm ns}}{(M_{\rm ns}M_{\rm bh}^2)^{1/3}}, \qquad (2)$$

is favorable. Thus, this simple estimate suggests that low masses for both the black hole and the neutron star are favorable.

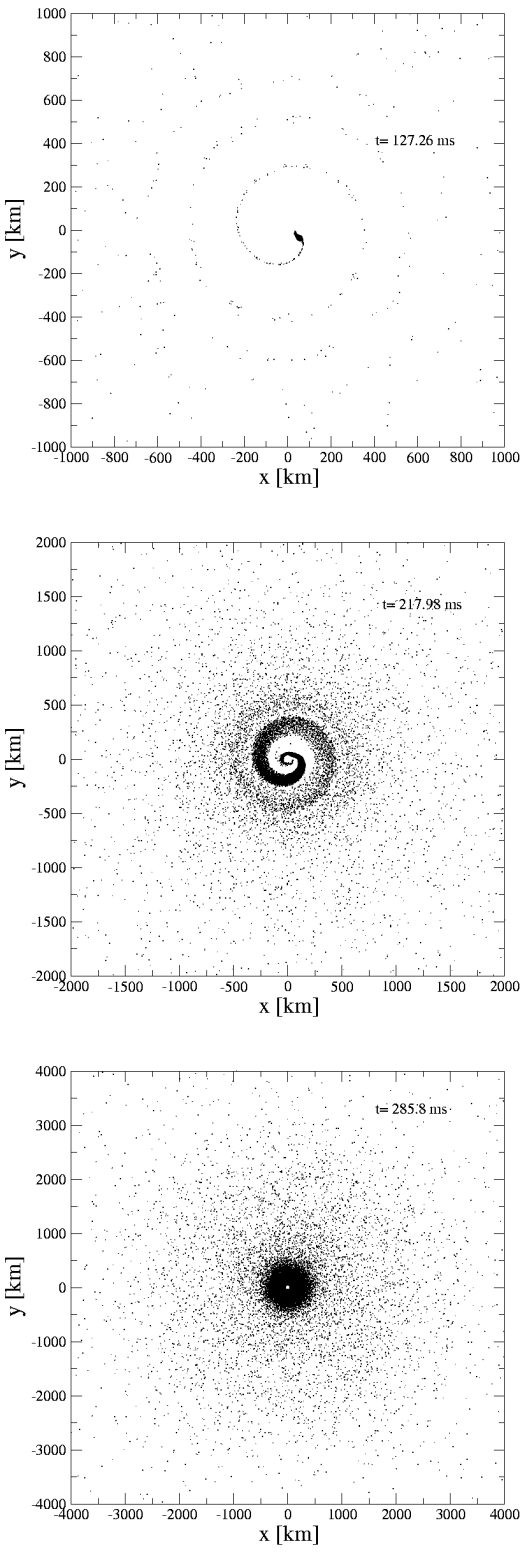

Fig. 6. Dynamical evolution of a neutron star black hole system that undergoes episodic mass transfer; continuation of Figure 5, left column.

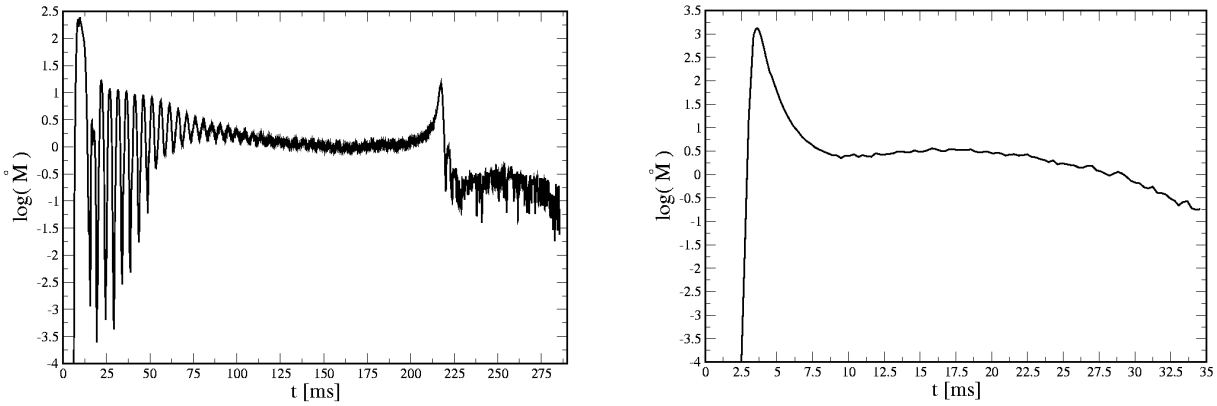

Fig. 7. Left panel: mass transfer (in $M_\odot$/s) into the black hole for the 1.4 $M_\odot$ and 3 $M_\odot$ system with episodic mass transfer (run NA in Table 1). Right panel: dito for the 1.4 $M_\odot$ and 14 $M_\odot$ system in which the neutron star is directly disrupted.

Taking together the calculations described in Rosswog (2005) and those of Table 1 the whole plausible black hole mass range from 3 to 20 $M_\odot$ (Fryer & Kalogera 2001) has been covered. For black holes below 10 $M_\odot$ Newtonian potentials and for more massive BHs Paczyński-Wiita (PW) pseudo-potentials have been used. To mimic the presence of a last stable orbit in the Newtonian calculations, we set up an absorbing boundary at $R_{\rm isco} = 6GM_{\rm BH}/c^2$. For the PW-potential matter is absorbed at $3GM_{\rm BH}/c^2$, for details see appendix in Rosswog (2005), but this material has passed the last stable orbit already and falls freely towards the hole, so the exact location of the boundary is unimportant. In all calculations a non-spinning neutron star mass with 1.4 $M_\odot$ was used.

For illustration, we want discuss two of the runs in more detail: A run with a 3 $M_\odot$ black hole (run NA in Table 1) as an example for a long-lived, episodic mass transfer, and a 14 $M_\odot$ run in which the neutron star is disrupted at during the first encounter.

2.2.1. *Episodic mass transfer*

In this calculation with a 3 $M_\odot$ black hole (run NA in Table 1) the neutron star undergoes a long-lived mass transfer without being disrupted, see Figure 5, left column. After a *primary mass transfer episode* with peak mass transfer rates beyond 100 $M_\odot$/s, see Figure 7, left panel, the neutron star recedes again and quenches the mass transfer. During this episode its mass is reduced to about 0.5 $M_\odot$, see right panel of Figure 8. Subsequently, it undergoes several more mass transfer episodes, after each episode mass transfer practically shuts off, leaving the neutron star constant for a short time (see "step-like" behaviour in the right panel of Figure 8). After about 25 episodes the mass transfer settles into a stationary state in which the neutron star transfers approximately 1 $M_\odot$/s directly into the hole without forming an accretion disk. Its general tendency during this episode is to move further away from the black hole, see left panel of Figure 8. Some material is tidally shed from the neutron star into a dilute disk around the still orbiting binary. It is only after 47 orbital periods, at t$\approx$ 218 ms, that the orbiting mini-neutron star becomes tidally disrupted and forms an accretion disk around the hole, see panels two and three in Figure 6. This final tidal disruption sets in when the mini-neutron star reaches its lower mass limit of about 0.18 $M_\odot$, see right panel of Figure 8 (for the mass radius relationship of the Shen et al. EOS see Fig. 1 in Rosswog et al. 2004).

This long-lived binary phase is imprinted on the gravitational wave signal, see Figure 9, left panel. The signal "chirps" until mass transfer sets in. The primary mass transfer episode reduces the gravitational wave amplitude by more than a factor of two. While the neutron star is constantly stripped by the black hole, the gravitational wave amplitude decreases until the minimum neutron star mass is reached. During this phase the binary emits at a frequency of $\approx$ 500 Hz, close to LIGO's sensitivity peak. This phase should be detectable out to a distance of $d = 10{\rm Mpc}(10^{-21}/h_{\rm min})$. Once this stage is reached, the gravitational wave signal shuts off abruptly as the matter settles quickly into an axisymmetric disk. During this final disruption, the mass transfer rate increases for a last time beyond 10 $M_\odot$/s, see the last pronounced peak around 200 ms in the left panel of Figure 7.

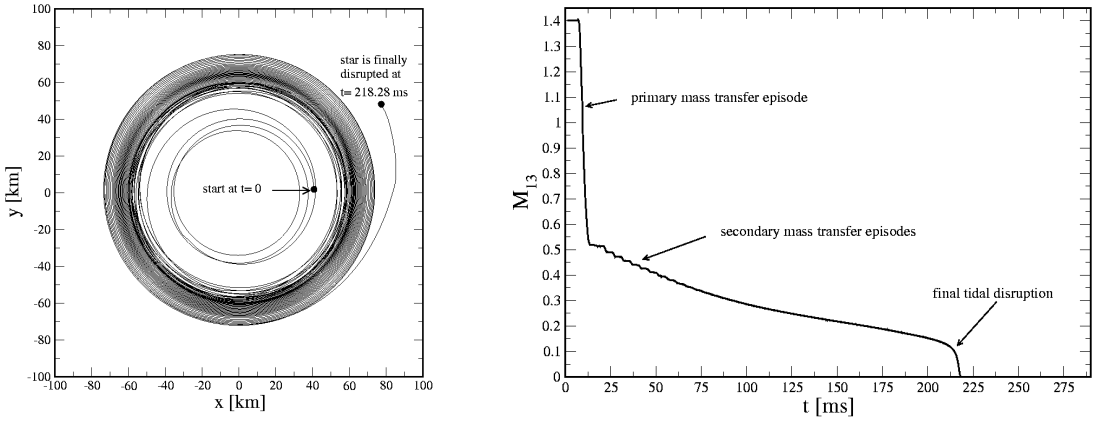

Fig. 8. Left panel: orbit of the mini-neutron star in the neutron star black hole system (M_{ns}=1.4 $M_\odot$, M_{bh}=3 $M_\odot$) that undergoes episodic mass transfer. After mass transfer has set in, the neutron star orbits the black hole for 47 orbital revolutions before it is finally disrupted. Right panel: elvolution of the neutron star mass (defined as the mass with $\rho > 10^{13}$ gcm^{-3}) of the same system.

2.2.2. *Direct disruption*

For more massive black holes, the self-gravity of the neutron star can be overcome already during the first, primary mass transfer. An example of such a case with a 14 $M_\odot$ black hole is shown in Figure 5, right column. Although the neutron star is disrupted, a density peak remains visible in the debris spiral arm until the end of the simulation. In this case an accretion disk forms, but large parts of this disk are inside the innermost stable circular orbit of the black hole and therefore falling with large radial velocities into the hole. This disks are geometrically thin and, apart from a spiral shock from the self-interaction of the accreted matter, essentially cold. A detailed discussion of this calculation can be found in Rosswog (2005). During the first approach mass is transferred into the black hole at a peak rate of more than 1000 $M_\odot$/s, see right panel of Figure 7.

Again the dynamics leaves a clear imprint on the gravitational wave signal: after the chirp stage the signal immediately dies off, see Figure 9 right panel. At peak amplitude, the signal should be visible out to $d = 250\mathrm{Mpc}(10^{-21}/h_{\min})$.

For the higher mass black holes, we do not find accretion disks that are promising to produce energetic GRBs. While some systems do form low-mass disks, see Figure 5, right column, for a 14 $M_\odot$ BH, for black holes with $M \geq 18\ M_\odot$, nearly the whole neutron star is directly fed into the hole, only a small fraction ($< 0.08\ M_\odot$) receives enough angular momentum to be ejected in form of a half-ring (see Fig. 3 in Rosswog 2005) of neutron-rich debris material.

2.3. *Constraints on the nuclear equation of state from gravitational waves*

As mentioned earlier, the neutron star equation of state (EOS) could be seriously constrained by a detected gravitational wave signal. We want to briefly summarize gravitational wave signatures that carry information on the nuclear EOS.

- A simple estimate for the neutron star radius can be obtained using Newtonian gravity and $\nu_{\rm GW} = 2\nu_{\rm orb}$, where $\nu_{\rm GW}$ and $\nu_{\rm orb}$ are the gravitational wave and orbital frequencies. If one assumes an equal mass binary, that the peak occurs once the neutron star surfaces touch and that changes due to tides are negligible, one finds

$$R_{\rm ns} = \left(\frac{GM}{8\pi^2\nu_{\rm p}^2}\right)^{1/3} = 16.8\ \mathrm{km}\ \left(\frac{M}{2.8\mathrm{M}_\odot}\right)^{\frac{1}{3}} \left(\frac{1\mathrm{MHz}}{\nu_{\rm p}}\right)^{\frac{2}{3}} . \quad (3)$$

  Here, $\nu_{\rm p}$ is the peak GW-frequency at the end of the chirp phase and M the total mass of the binary. More accurately, using quasi-equilibrium sequences of neutron star binaries, the compactness GM/Rc^2 can be determined from the final deviation of the gravitational wave energy spectrum from a point mass binary signal (Faber et al. 2002). If additionally the neutron star masses are known from the inspiral signal (Cutler & Flanagan 1994), the neutron star radius can be derived and severe constraints on the equation of state can be imposed.

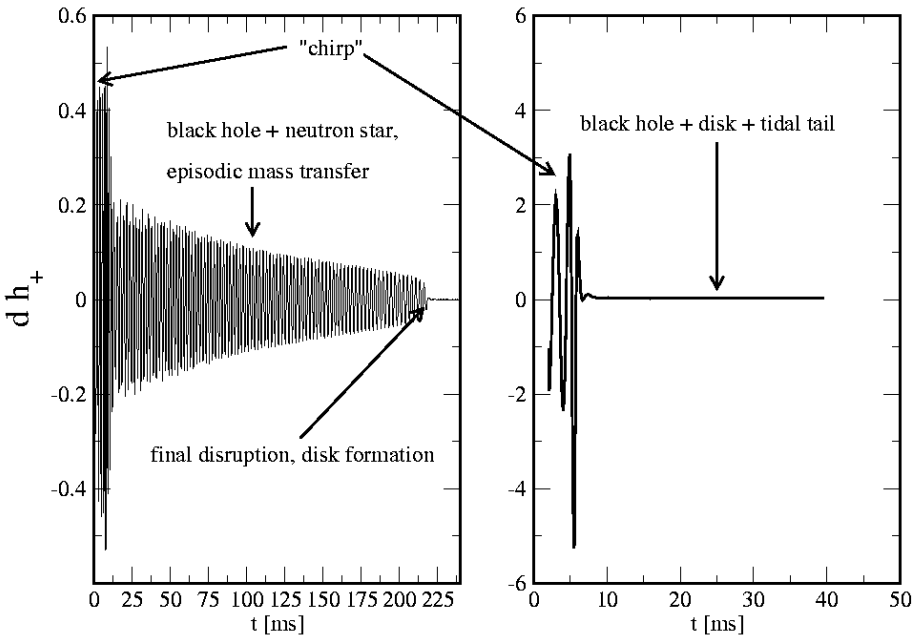

Fig. 9. Left panel: gravitational wave signal of a binary system that undergoes episodic mass transfer (M_{ns}=1.4 $M_\odot$, M_{bh}=3 $M_\odot$). Right panel: gravitational waves for the 1.4 $M_\odot$ and 14 $M_\odot$ system in which the neutron star is directly disrupted (run II of Rosswog 2005).

- The stiffness of the EOS influences the post-merger behaviour of the remnant. If the EOS is stiff enough, the central object will keep a triaxial, ellipsoidal shape for many orbital periods and thus will continue to emit gravitational waves (e.g. Rasio & Shapiro 1994), before it (probably) finally collapses into a black hole. For a soft EOS it will quickly become axisymmetric and the GW-signal will die off fast. The influence of quark matter on the gravitational wave signal has recently been investigated by Oechslin et al. (2004).
- As was shown in Section 2.2.1, NSBH systems with low black hole masses can undergo a long-lived (in comparison to orbital time), mostly episodic mass transfer activity. Test calculations with a soft ($\Gamma = 2$) polytrope (Rosswog et al. 2004) indicate that this behaviour is specific for stiff equations of state. Moreover, from a gravitational wave signal such as the one shown Figure 9, left panel, the time when the neutron star reaches its minimum mass can be directly read off: at this point the gravitational wave signal suddenly shuts off.

3. ACCRETION DISKS

The accretion disks produced in a compact binary merger are in several respects different from a standard Shakura-Sunyaev (1973) accretion disk. Having just been built up in a violent disruption, they are far from a steady state and completely opaque to photons. Cooling is only possible via neutrino emission. The corresponding processes, however, are not generally fast enough to cool the disks on a timescale comparable to the dynamical timescales. The disks often span the full range from neutrino opaque to completely transparent with relatively large semi-transparent transition regions making an analytical treatment without restrictive assumptions difficult. Over the last years several groups have worked in different approximations on the neutrino-cooled disk problem (e.g. Popham et al. 1999; Narayan, Piran, & Kumar 2001; Kohri & Mineshige 2002; DiMatteo et al. 2002). Recently, equilibrium disks around rotating black holes have been constructed by Chen & Beloborodov (2006). Neutrino opacity effects have been included in several of the recent numerical simulations (Ruffert et al. 1997; Rosswog & Liebendörfer 2003a; Lee et al. 2005).

3.1. *Double neutron star mergers*

We show in Figure 10 disk properties of run DA that we consider representative for the DNS case. The dominant neutrino-emitting parts of the disks have densities in the range from $\sim 10^{13}$ down to

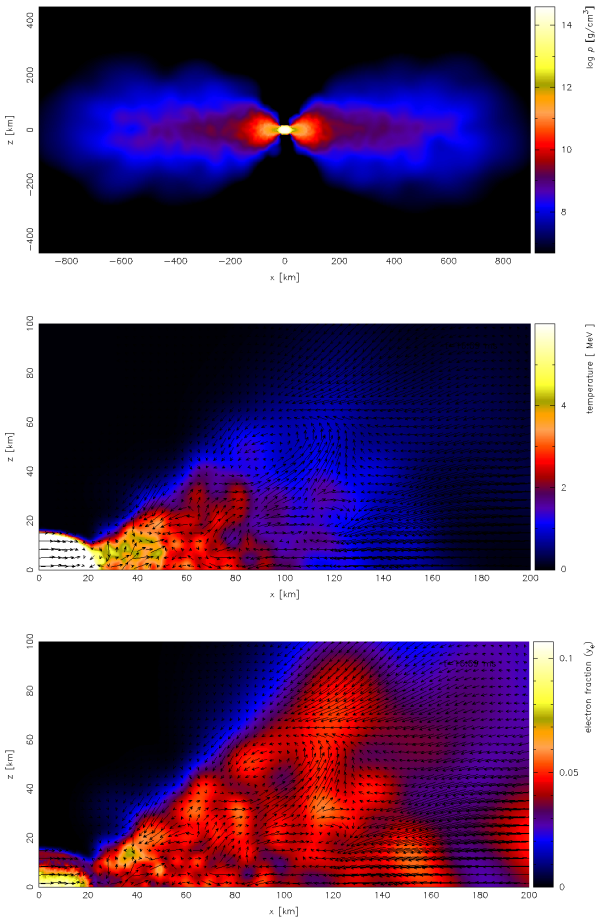

Fig. 10. Vertical structure of the debris disk resulting from an equal mass (1.4 $M_\odot$) double neutron star merger (run DA, see Table 1, at t= 16.88 ms). Panel one shows the global mass density distribution in the XZ-plane; panel two zooms into inner disk region, color-coded is the temperature. To enhance the temperature contrasts in the disk the upper limit of the colorbar has been fixed to 6 MeV. Panel three shows the distribution of the electron fraction, Y_e; in panels two and three the velocity field is overlaid.

$\sim 10^{10}$ gcm^{-3}, see panel one, the temperatures in these regions are $\sim$ 3 MeV. At the time of the merger, the neutron stars are still very close to cold β-equilibrium as the tidal interaction is too short to cause substantial compositional changes at the prevailing temperatures ($T < 10^8$ K; Lai 1995). The weak interaction rates during the merger are sufficiently slow that the matter in the remnant is at $\sim$ 15 ms still close to its initial electron fraction, $Y_e \sim 0.05$, see panel three in Figure 10. Therefore the assumption of β-equilibrium is not justified.

The central object is apart from its surface layers completely opaque to the neutrinos. The inner parts of the debris torus still have large optical depths, see Figs. 8-10 in Rosswog & Liebendörfer (2003a), only the outer parts are neutrino transparent. As the disks cannot cool on a dynamical timescale they are puffed-up and advection dominated. Inflow towards the central object proceeds mainly along the equatorial plane (see arrows in panel two and three) and along the disk surface, the flow inside the disks shows convective circulation. For a further discussion of the circulation patterns see Lee & Ramirez-Ruiz (2002); Rosswog & Davies (2002a) and Lee et al. (2005).

3.2. *Neutron star black hole mergers*

In the neutron star black hole case we find it much harder to build up massive accretion disks. In the low-mass cases the episodic mass transfer prevents disk formation until the neutron star is finally disrupted once it has been stripped down to its minimum mass of about 0.18 $M_\odot$. Such a case was shown in detail in Figures 5 and 6. The resulting disk as seen in panel six of Figure 6 has about 0.05 $M_\odot$. For the cases with larger black hole mass, the neutron star is completely disrupted early on, see Section 2.2.2, but close to the innermost stable circular orbit. As a consequence, matter falls with large radial velocities into the hole within about one orbital period. These disks are essentially cold (apart from a spiral shock that occurs due to self-interaction of the accretion stream, see Fig. 6 in Rosswog 2005), low in density and, contrary to the neutron star merger disks, they are geometrically thin. For even higher black hole masses the neutron star is nearly swallowed completely without any disk formation. For a further discussion we refer to Rosswog (2005).

These result seems to depend on the nuclear equation of state. Janka et al. (1999) who use the softer Lattimer-Swesty EOS find disks that are more promising for GRBs.

To quantify the amount of present debris material for both the DNS and the NSBH cases, we use the mass that is gravitationally bound and has a density $\rho < 10^{13}$ gcm^{-3}. The evolution of this debris mass is shown in Figure 11. In the DNS cases the debris mass is around 0.3 $M_\odot$, for the black hole cases it is about one order of magnitude smaller, at maximum $\approx$ 0.05 $M_\odot$. In run NA, which is described in detail in Section 2.2.1, the mass transfer is constantly driving neutron star oscillations, see Figure 11, right panel. The debris mass only increases beyond 0.01 $M_\odot$ after the neutron star is completely disrupted at t$\approx$ 218 ms.

To further illustrate the different thermodynamic condition prevailing in the debris of DNS and NSBH

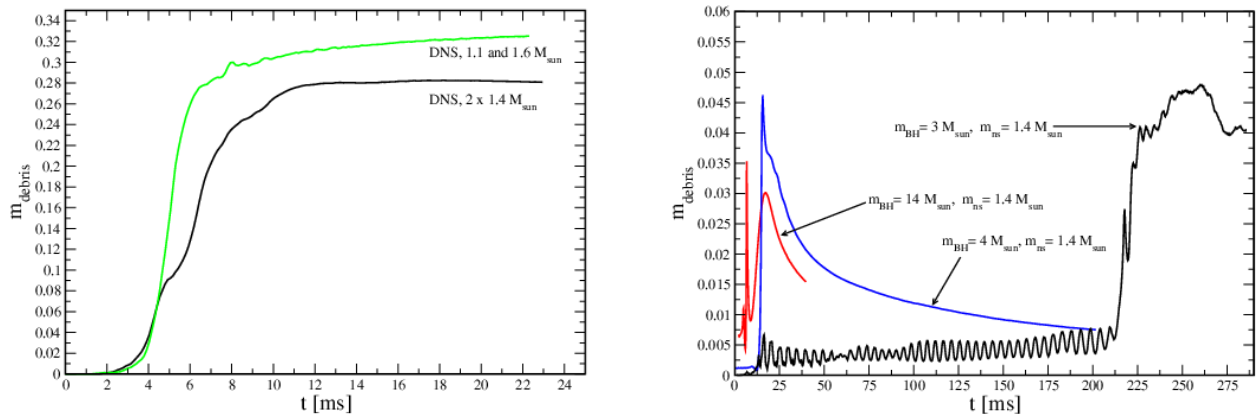

Fig. 11. Comparison between double neutron star and neutron star black hole mergers. Left panel: debris mass (gravitationally bound, $\rho < 10^{13}$ gcm^{-3}) for the double neutron star case. Right panel: debris mass for the neutron star black hole cases. Note the different scales on the axes of both panels.

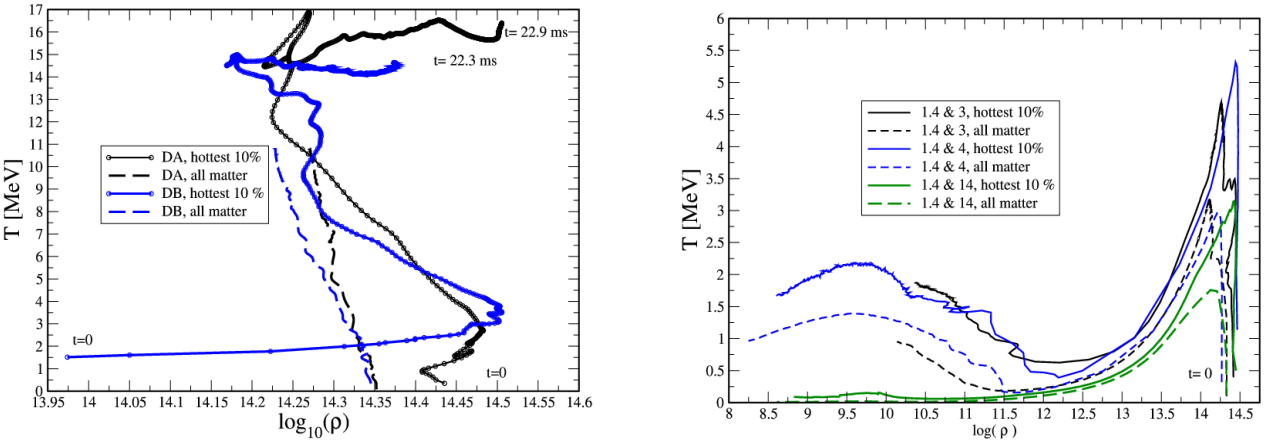

Fig. 12. Comparison between double neutron star and neutron star black hole mergers. Left panel: Trajectories in the $\rho - T$-plane for double neutron star cases (run DA and DB). Right panel: typical neutron star black hole cases. For each case, the trajectories of the hottest 10% of the material and an average over all matter are shown.

remnants, we show in Figure 12 trajectories in the $\rho - T$-plane. The left panel refers to the two neutron star cases, the right panel shows typical trajectories of NSBH systems. The solid lines always refer to the average of the hottest 10% of the debris, the dashed lines show the average conditions of all matter. While in the neutron star case the hottest material is always at very high densities ($> 10^{14}$ gcm^{-3}), the hottest regions in the NSBH cases move during the evolution down to densities of $\leq 10^{10}$gcm^{-3}and below. In the direct disruption case that was discussed in Section 2.2.2, the average temperature of even the hottest 10% of the material quickly drops below 1 MeV (solid green curve).

4. NEUTRINO EMISSION

4.1. *Double neutron stars*

The debris in the DNS case is very neutron-rich and hot, so the neutrino luminosities are generally dominated by electron anti-neutrinos from positron captures onto free neutrons, $e^+ + n \rightarrow p + \nu_e$. Electron neutrinos, mainly from electron captures, $e + p \rightarrow n + \bar{\nu}_e$, are second most important and followed by the heavy lepton neutrinos $\nu_\mu, \bar{\nu}_\mu, \nu_\tau, \bar{\nu}_\tau$ that we generally refer to as ν_x. While the ν_e and $\bar{\nu}_e$ are emitted predominantly from the inner disk regions or the surface layers of the central object, the heavy lepton neutrinos ν_x are mainly produced in

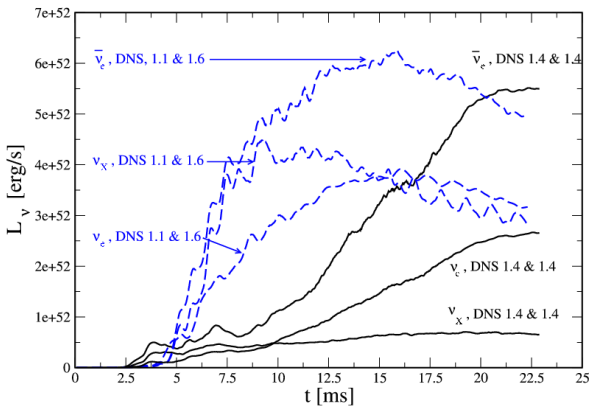

Fig. 13. Neutrino luminosities of the double neutron star merger cases. Solid lines refer to the case with $2\times1.4\ M_\odot$, the dashed lines to the 1.1 and 1.6 $M_\odot$case.

the hot high-density regions inside the central object. Since the heavy lepton neutrinos are not absorbed by nucleons, the surrounding matter is more transparent to them. Therefore, they can escape from the hotter, high density regions more easily, which is why they have the largest average energy. The average energies of the neutrino species are relatively robust against changes in the system parameters, typically $\langle E_{\nu_e}\rangle \approx 7$ MeV, $\langle E_{\bar{\nu}_e}\rangle \approx 12$ MeV and $\langle E_{\nu_x}\rangle \approx 23$ MeV. In the unlikely case that neutrinos from a neutron star merger would be detected, the substantial drop in the ν_x, but only a milder drop in the ν_e and $\bar{\nu}_e$ luminosity would indicate the moment when the central objects collapses into a black hole.

The neutrino luminosities after a DNS merger increase smoothly until a stationary state is reached, see Figure 13. At this stage the luminosities of the numerical models can be roughly fit by

$$L_\nu^{tot} = L_1 \left(\frac{M}{2.6\ \mathrm{M}_\odot}\right)^\alpha \qquad (4)$$

with $L_1 = 6.8\cdot10^{52}$ erg/s, $\alpha = 4.5$ and M being the total binary mass. This formula does not apply to cases where an Algol-like impact occurs (run DB), in such a case the neutrino-luminosities are higher due to the very strong shock heating at moderate densities. The contribution of the different neutrino flavors to the total luminosity changes with the details of the system under consideration, but they are approximately given by $L_{\nu_e} \approx 0.3\cdot L_\nu^{tot}$, $L_{\bar{\nu}_e} \approx 0.5\cdot L_\nu^{tot}$ and $L_{\nu_x} \approx 0.2\cdot L_\nu^{tot}$.

The disks that were produced in neutron star black hole calculations were only of moderate masses and temperatures and therefore produced much lower luminosities than in the neutron star case. Calculations with the softer EOS of Lattimer & Swesty (1991) and Janka et al. (1999), find results not too different from the DNS case.

5. GRBS

Compact binary mergers have been recognized as possible central engines of GRBs since many years (Blinnikov et al. 1984; Eichler et al. 1989; Paczyński1991; Narayan et al. 1991). For general reviews on the manifold aspects of gamma-ray bursts we refer to recent reviews (e.g. Piran 2005 or Mészáros2006).

To attain the ultra-relativistic motion required to explain both the short-time variability and the non-thermal spectrum of GRBs, large amounts of energy have to be deposited in a region of space that is practically devoid of baryons. Two popular mechanisms to achieve this are the annihilation of neutrino anti-neutrino pairs (Eichler et al. 1989; Mochkovitch et al. 1993; Ruffert et al. 1997; Popham et al. 1999; Asano & Fukuyama 2003; Rosswog & Ramirez-Ruiz 2002b; Rosswog et al. 2003c) and mechanisms that rely on (ultra-)strong magnetic fields (Narayan et al. 1991; Usov 1992; Duncan & Thompson 1992; Thompson 1994; Mészáros& Rees 1997; Kluzńiak & Ruderman 1998; Lyutikov et al. 2003; Rosswog et al. 2003c).

5.1. $\nu_i - \bar{\nu}_i$-annihilation

The energy deposition rate per volume via neutrino anti-neutrino annihilation (see Ruffert et al. 1997) can be written is discretised form as

$$\begin{aligned} Q_{\nu\bar{\nu}}(\vec{r}) &= \sum_{i=e,\mu,\tau} Q_{\nu_i\bar{\nu}_i}(\vec{r}) \\ &= \sum_{i=e,\mu,\tau} A_{1,i} \sum_k \frac{L^k_{\nu_i}}{d_k^2} \sum_{k'} \frac{L^{k'}_{\bar{\nu}_i}}{d_{k'}^2} [\langle E_{\nu_i}\rangle^k + \langle E_{\bar{\nu}_i}\rangle^{k'}] \mu^2_{kk'} \\ &+ \sum_{i=e,\mu,\tau} A_{2,i} \sum_k \frac{L^k_{\nu_i}}{d_k^2} \sum_{k'} \frac{L^{k'}_{\bar{\nu}_i}}{d_{k'}^2} \frac{\langle E_{\nu_i}\rangle^k + \langle E_{\bar{\nu}_i}\rangle^{k'}}{\langle E_{\nu_i}\rangle^k \langle E_{\bar{\nu}_i}\rangle^{k'}} \mu_{kk'} \qquad (5) \end{aligned}$$

where the index i labels the type of neutrino. Here L^k is the neutrino luminosity of grid cell k, d_k is the distance from the centre of grid cell k to the point $\vec{r}$, $d_k = |\vec{r} - \vec{r}_k|$, $\langle E_{\nu_i}\rangle^k$ is the average neutrino energy in grid cell k, $\mu_{kk'} = 1 - \cos\theta_{kk'}$ and $\theta_{kk'}$ is the angle at which neutrinos from cell k encounter anti-neutrinos from cell k' at the point $\vec{r}$. The constants are given by $A_{1,e} = \frac{1}{12\pi^2}\frac{\sigma_0}{c(m_e c^2)^2}[(C_V - C_A)^2 + (C_V + C_A)^2]$, $A_{1,\mu} = A_{1,\tau} = \frac{1}{12\pi^2}\frac{\sigma_0}{c(m_e c^2)^2}[(C_V - C_A)^2 + (C_V + C_A - 2)^2]$, $A_{2,e} = \frac{1}{6\pi^2}\frac{\sigma_0}{c}[2C_V^2 - C_A^2]$, $A_{2,\mu} = A_{2,\tau} = \frac{1}{6\pi^2}\frac{\sigma_0}{c}[2(C_V - 1)^2 - (C_A - 1)^2]$, where $C_V = 1/2 + 2\sin^2\theta_W$, $C_A = 1/2$, $\sin^2\theta_W = 0.23$ and $\sigma_0 = 1.76\times10^{-44}\mathrm{cm}^2$.

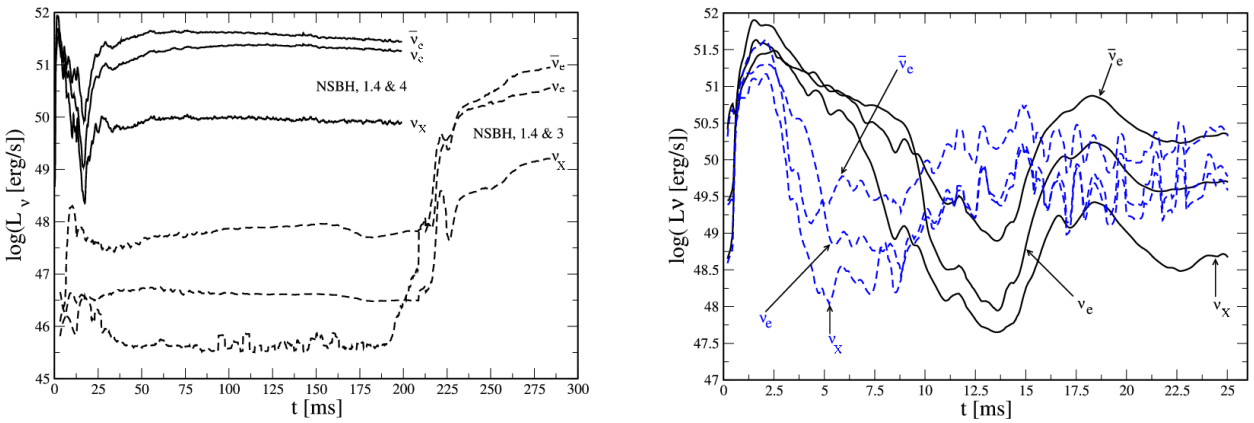

Fig. 14. Neutrino luminosities of the neutron star black hole cases. Left panel: black holes with 3 (dashed) and 4 $M_\odot$ (solid curves). Right panel: black holes with 7 (solid) and 10 $M_\odot$ (dashed curves).

The thick-disk geometry that is a natural outcome of a double neutron star merger, see Figure 10, is favorable for an efficient annihilation as neutrinos have enhanced probability to collide head-on. The most interesting regions for the energy deposition are the centrifugally baryon-cleaned regions along the original binary rotation axis. Contours of the matter density and the annihilation energy deposition rate can be found in Fig. 2 in Rosswog et al. (2003c). The deposition of a large amount of energy in a photon-pair plasma between the funnel walls results in a bipolar outflow along the binary rotation axis. The ratio of deposited annihilation and rest mass energy determines the asymptotic Lorentz-factors of the resulting outflow. For a double neutron star merger these Lorentz-factors lie between a few dozens and a few times 10^4 (see Rosswog et al. 2003c, Figs. 4-6). The total energy contained in this relativistic outflow is $\sim 10^{48}$ erg (Rosswog & Ramirez-Ruiz 2003b).

Similar to the case of a new-born proto-neutron star, the huge neutrino luminosity will also drive an energy baryonic winds off the remnant. The interaction with the baryonic material collimates the neutrino-annihilation-driven bipolar outflow. Using simple estimates Rosswog & Ramirez-Ruiz (2003b) found a broad distributions of opening angles and isotropised luminosities, centered around 7° and a few times 10^{50} erg, respectively.

More recently, Aloy, Janka, & Müller (2005) have performed detailed, axisymmetric relativistic hydrodynamic simulations in which they parametrised the energy deposition above remnant accretion disks. Some of their models did not produce ultra-relativistic outflows and instead lead to low-luminosity UV-flashes, others were able to produce ultra-relativistic, structured outflows that are promising GRBs sources. While the ultimate outcome seems to depend quite sensitively on the details of the considered system (disk structure, energy deposition rates, injection duration), their most promising systems produced ultra-relativistic outflows with half-opening angles of 5-10° and apparent isotropic energies of up to 10^{51} erg.

It has to be stressed that to date no self-consistent calculations of a full merger with neutrino emission, annihilation, launch of winds and relativistic outflow could be performed. Only individual aspects have been simulated that are a posteriori patched together into a global picture. Nevertheless, the theoretical numbers found in the last two investigations are consistent with recent observations of short GRBs that find values of E_γ of a few times 10^{48} erg and opening half-angles from about 9 to about 14° (Fox et al. 2005; Berger et al. 2005). Note however, that there are recent observations (Berger et al. 2006b) that suggest that a fraction of short GRBs may have substantially larger energies than the first few short bursts that were detected.

Thus, neutrino annihilation from compact merger remnants, at least in the DNS case, seems to be in reasonable agreement with recent observations of short GRBs.

5.2. *Magnetic fields*

Nevertheless, it is hard to see how magnetic fields should not play an important role. Most neutron stars are endowed with strong magnetic fields: young pulsars typically have $\sim 10^{12}$ G and magnetars (Duncan & Thompson 1992) are thought to have magnetic fields between 10^{14} and 10^{15} G. While

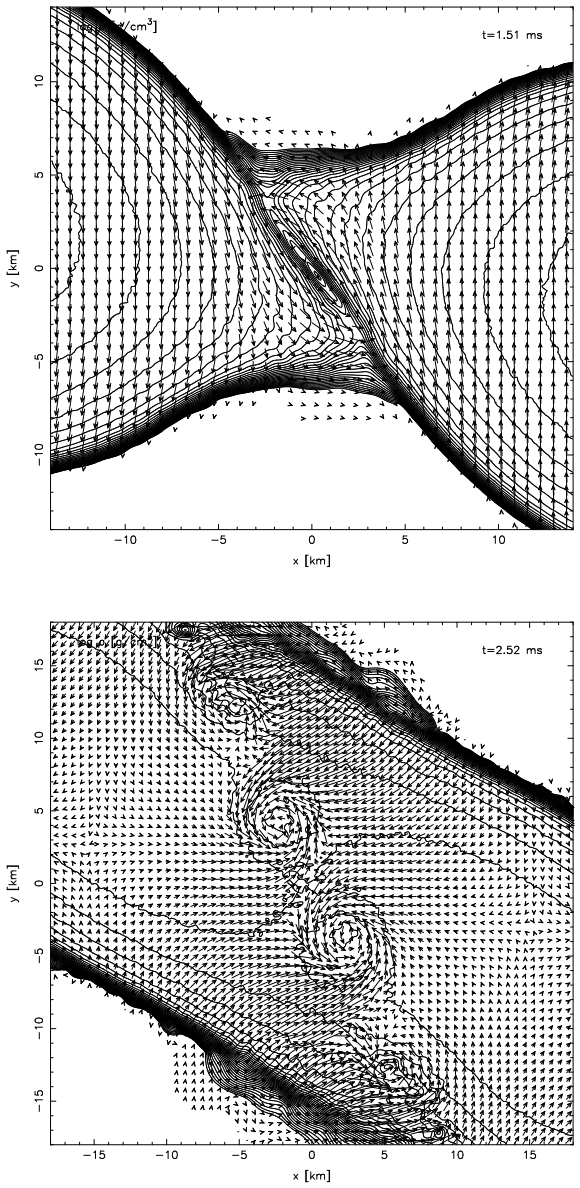

Fig. 15. Velocity fields during the merger of two 1.4 $M_\odot$ neutron stars (run DA). The shear interface, see panel one, becomes Kelvin-Helmholtz unstable and forms a string of vortex rolls (panel two, velocities in corotating frame) in which the magnetic field is curled up.

still more speculative than the neutrino annihilation mechanism in the sense that the existing calculations are less detailed, there are good arguments to expect a dramatic growth of existing seed fields.

The merger debris is differentially rotating, both the central object before collapse, see Fig. 9 in Rosswog & Davies (2002a), and the surrounding disk.

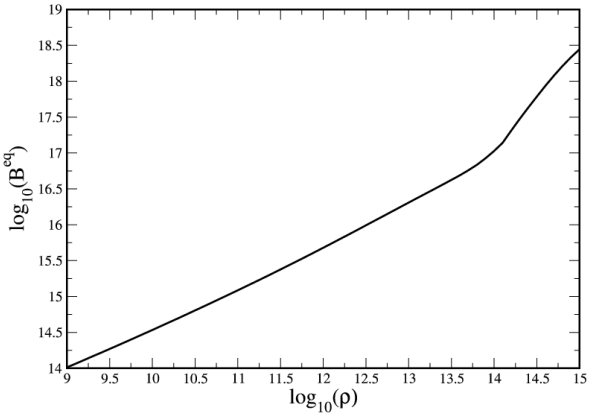

Fig. 16. Field strength (in G), where the magnetic pressure, equals the matter pressure (calculated from the Shen et al. EOS (1998) with $T = 0.5$ MeV and $Y_e = 0.1$).

Thus the initial seed fields can grow either just by a linear winding up the field lines or, more likely, via the magnetorotational instability (MRI) (e.g. Balbus & Hawley 1998). Recent magnetohydrodynamics simulations (Price & Rosswog 2006) suggest that magnetic seed fields are rapidly amplified in the Kelvin-Helmholtz instability at the shear interface between the two neutron stars, see Figure 15. This amplification occurs on a timescale of only ~ 1 ms, long before the collapse can set in. As the shortest modes grow fastest in a Kelvin-Helmholtz instability, the reached maximum field strengths are limited by the finite numerical resolution. At the highest affordable resolution, about $2 \cdot 10^{15}$ G are reached, but very plausibly *much* higher field strengths will be realized in nature. The kinetic energy of the central object is large, about $8 \cdot 10^{52}$ erg, and if say 10 % of this energy can be transformed into magnetic field energy, the field strength averaged over the central object will be in excess of 10^{17} G. Locally, the field could be substantially higher.

To become dynamically important, the fields have to become extremely strong. The field strengths at which the magnetic pressure balances the nuclear matter pressure are shown in Figure 16. In the central object of a merger these field strengths are in excess of 10^{17} G, in the accretion disk they are still between 10^{14} and 10^{16} G. If the central object remains stable for long enough, it could provide a Poynting-dominated, scaled-up relativistic pulsar wind. In this case energy is released at a rate of

$$\left(\frac{dE}{dt}\right)_{\rm md} \sim 10^{51} B_{16}^2 P_{\rm ms}^{-4} R_6^6 \ {\rm erg/s} \qquad (6)$$

and the central object will spin down on a timescale given by

$$\tau_{\rm sd} \sim 2{\rm s}\, B_{16}^{-2} P_{\rm ms}^2 \left(\frac{20\ {\rm km}}{R_{\rm co}}\right)^4 \left(\frac{M_{\rm co}}{2.5\ {\rm M}_\odot}\right), \qquad (7)$$

where B_{16} is $B/10^{16}$G and $P_{\rm ms} = P/1$ ms.

Fluid instabilities, such as the Kelvin-Helmholtz instability illustrated for run DA in Figure 15, will locally curl up the magnetic field lines. This had been suggested earlier (Rosswog et al. 2003c) and has recently been confirmed by first MHD-merger simulations (Price & Rosswog 2006). Once such high-field pockets reach field strengths close the equipartition, see Figure 16, they will become buoyant, float up and produce explosive reconnection events (e.g. Kluzńiak & Ruderman 1998; Rosswog et al. 2003c). This may also occur in the disk (e.g. Narayan et al. 1991), though at a lower field strength, see Figure 16. Once the central object has collapsed, the "standard GRB-engine", a black hole plus accretion torus, remains, for which various energy extraction mechanisms have been suggested (e.g. Blandford & Znajek 1977; Blandford & Payne 1982; or McKinney 2005). For a discussion of these mechanisms we refer to the literature.

As discussed in the previous sections in our neutron star black hole calculations we find it difficult to form massive disks. The neutrino luminosities are even in the more optimistic cases two orders of magnitude lower than in the DNS case, see Figures 13 and 14. This is mainly due to the much smaller debris mass, see Figure 11. As the neutrino annihilation roughly scales with the square of the neutrino luminosity, see Eq. (5), neutrino annihilation deposits substantially less energy than in the DNS case. NSBH binaries would therefore not produce energetic GRBs, but rather a low-luminosity tail to the short GRB distribution. Possible observable signals are discussed in Rosswog (2005).

We want to stress again that these results are sensitive to the nuclear EOS. With the softer Lattimer-Swesty-EOS Janka et al. (1999) find more promising conditions.

6. FORMATION OF A MAGNETAR?

There are essentially two proposed formation mechanisms for pulsars: i) the collapse of very rapidly rotating stars with ordinary magnetic fields or ii) the collapse of extraordinarily magnetized stars with ordinary rotational speeds. In the first case the new-born proto-neutron star has to be rotating rapidly enough so that rotational periods are smaller than the overturn times, ~ 3 ms, of convective eddies (Duncan & Thompson 1992; Thompson & Duncan 1993, 1995), so that an efficient α-ω-dynamo can become active. In this way, fields as strong as $\sim 10^{15}$ G can be plausibly generated. Such a new-born neutron star will be spun down quickly by magnetic dipole radiation (and possibly mass loss) and this will fuel the supernova explosion with an additional $2\pi^2 I/P^2 \sim 2 \cdot 10^{52} I_{45}/P_{\rm ms}^2$ ergs stemming from rotational energy. Here we have used I_{45}, the moment of inertia in units of $10^{45}{\rm gcm}^2$ and $P_{\rm ms}$, the rotation period as measured in milliseconds. Therefore, particularly bright supernova explosions going along with magnetar formation are a natural prediction of this formation path. However, the three supernova remnants that seem to be associated with magnetars are remarkably unremarkable: rather than being particularly energetic they only have kinetic energies of $\sim 10^{51}$ ergs (Sasaki et al. 2004; Vink 2006). An alternative formation scenario could be that the magnetar field strengths are obtained via magnetic flux conservation alone during the collapse of highly magnetized progenitor stars (Ferrario & Wickramasinghe 2005).

Here, we want to discuss a third possible formation channel, namely a neutron star coalescence that produces produces a stable, magnetar-like remnant.

The first point to clarify is whether the DNS merger rates are large enough to possibly contribute a non-negligible fraction of magnetars. The estimated rates at which double neutron systems (DNS) merge have been constantly increasing over the last years. The discovery of the double pulsar PSR J0737-3039A (Burgay et al. 2003) alone has increased the estimated merger rate based on observational data by an order of magnitude. Current estimates (Kalogera et al. 2004) are in the range from 4 to 224 $\cdot 10^{-6}$ per year and Galaxy. Nakar et al. (2006) based their estimates on the assumption that short-hard gamma-ray bursts result from DNS mergers. They find a "best guess" value that is higher than the above upper limit by more than an order of magnitude. This last rate may be somewhat optimistic, but it is fair to state that the DNS merger rate is comparable to the magnetar birthrate in our Galaxy, about 1-10 $\cdot 10^{-4}$ per year (Duncan & Thompson 1992). DNS mergers could therefore plausibly contribute to the magnetar production.

The main question that needs to be addressed is whether the final remnant of a DNS merger can have a mass that can be permanently sustained by the equation of state. The maximum neutron star mass is unfortunately still only poorly constrained. An upper limit based on very general physical prin-

ciples such as causality is 3.2 $M_\odot$(Rhoades & Ruffini 1974)[3]. In a review of realistic models of nuclear forces Akmal et al. (1998) find that realistic models of nuclear forces limit the maximum mass of neutron stars to be below 2.5 $M_\odot$. The masses with the smallest error bars come from the observation of DNS and they are consistent with a remarkably narrow underlying Gaussian mass distribution with M=1.35±0.04 $M_\odot$ (Thorsett & Chakrabarty 1999). Observations of neutron stars in binary systems with a white dwarf, however, yield consistently higher neutron star masses, but the error bars are to date still much larger than in DNS. The most extreme case is PSR J0751+1807 with an estimated pulsar mass of 2.1 ± 0.2 $M_\odot$ (Nice et al. 2005). Recent observations of the neutron star EXO 0748-676 also seem to support large possible neutron star masses and have been interpreted as hints that neutron stars may have a conventional neutron-proton composition (Özel 2006). Here, we want to explore the possibility that the final outcome of a DNS coalescence is, after some mass loss, a very massive and highly magnetised, but stable neutron star.

Let us first estimate the gravitational mass of a merger remnant. Lattimer & Yahil (1989) found empirically that

$$B = \alpha \left(\frac{M}{M_\odot} \right)^2, \quad (8)$$

with $\alpha = 0.084$ $M_\odot$, yields a good fit of the binding energy, B, as a function of the gravitational mass M. Thus, a standard binary system of twice 1.35 $M_\odot$ corresponds to a baryonic mass of about 3.0 $M_\odot$, or, a merger remnant made of all the baryons of the initial binary system would have 2.48 $M_\odot$ of gravitational mass.

We plot in Figure 17 the baryonic mass that needs to become unbound in order for the final remnant to be above a specified maximum neutron star mass $\mathrm{M_{max}}$:

$$m_{\rm loss} = 2(\alpha M_{\rm ns}^2 + M_{\rm ns}) - (\alpha M_{\rm max}^2 + M_{\rm max}), \quad (9)$$

where we have restricted ourselves to the case of equal mass neutron stars. For example, if we assume the maximum neutron star mass to be 2.2 $M_\odot$, so just beyond the estimated mass of PSR J0751+1807, a system with two 1.2 (1.4) $M_\odot$ neutron stars would need to loose a baryonic mass of 0.035 (0.52) $M_\odot$.

Mass can be lost by dynamical ejection or by the combined action of neutrinos, rotation and strong magnetic field as a neutrino-magnetocentrifugally driven outflow. The latter mechanism has been discussed recently (Thompson, Chang, & Quataert 2004) in the context of the formation of magnetars in supernovae.

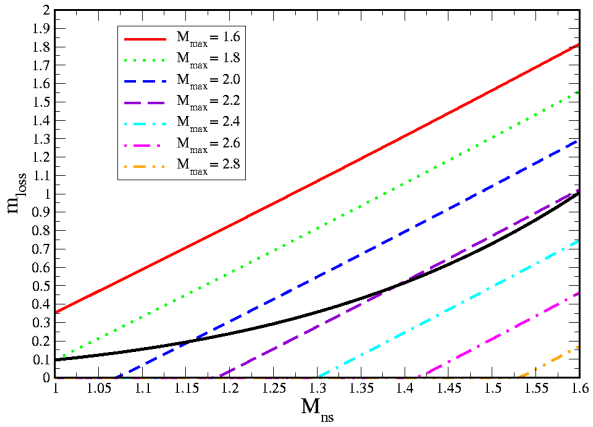

Fig. 17. Shown is the baryonic mass that has to be lost from a double neutron star system with twice M_{ns} if the maximum gravitational neutron star mass is $M_{\rm max}$. All masses are in solar units. The black solid curve is the estimate of the mass that is lost by the neutrino-magnetocentrifugal wind plus dynamic ejection, see text.

The amount of mass that is *dynamically* ejected is sensitive to the nuclear equation of state (EOS) with stiffer EOSs ejecting more than softer ones (Rosswog et al. 2000). With the EOS of Shen et al. (1998), which is at the stiffer end of the EOS spectrum and therefore consistent with the assumption of a relatively large maximum neutron star mass, we find that typically $m_{ej} \approx 0.03$ $M_\odot$ are dynamically ejected.

The combined action of neutrino-heating, strong magnetic field and rapid rotation is hard to quantify as details of the (unknown) magnetic field geometry enter and the mass loss rates depend sensitively on the neutrino luminosity and the rotational period (Duncan et al. 1986; Qian & Woosley 1996; Thompson et al. 2001, 2004). Strong magnetic fields enforce near-corotation of the wind with the stellar surface out to the Alfven radius, R_A, where the kinetic enery, $\rho v^2/2$ approximately equals the magnetic energy density $B^2/8\pi$. Thus, wind mass elements are, like spokes on a bike wheel, forced to corotate with the remnant, leading much faster loss of angular momentum and spin-down. Thompson et al. (2004) find that a strong magnetic field together with the rapid rotation will *drastically* increase the mass loss rate, in the fast-rotation limit they find a functional dependence of

$$\dot{M} \propto \exp(\omega^2), \quad (10)$$

[3]See Psaltis (2006) for a critical analysis of the underlying assumptions.

where ω is the angular frequency. This indicates that a substantial mass loss is possible. For example, for a central remnant period of 0.8 ms (see Fig. 10 in Rosswog & Davies 2002a) and a neutrino luminosity of $L_{\bar{\nu}_e} = 8 \cdot 10^{51}$ erg/s they find a mass loss rate $\dot{M} \approx 0.1\ M_\odot$ /s. If we assume that the results scale like $\dot{M} \propto L_\nu^{2.5} M^{-2}$ (Qian & Woosley 1996) and use the empirical relation Equation (4), we can estimate $\dot{M}$ as a function of the total mass of the DNS, M. This is shown as the solid black line in Figure 17 for a duration of $\tau = 0.5s$, the total unbound mass being $m \sim \dot{M} \cdot \tau + m_{ej}$. Taking these numbers at face value would mean that, if the maximum neutron star mass is $M_{\rm max} = 2.2\ M_\odot$ (violet line in Figure 17), then even a standard DNS with twice 1.35 $M_\odot$ would loose enough mass to leave a stable remnant. For $M_{\rm max} = 2.0\ M_\odot$ (blue), neutron stars with or below 1.15 $M_\odot$ would still produce a stable neutron star.

To summarize, although hard numbers are difficult to obtain, the lower end of the DNS mass distribution could plausibly produce stable, highly magnetized neutron stars rather than black holes.

7. LATE-TIME CENTRAL ENGINE ACTIVITY

It was one of the surprises of the recent afterglow detections of short GRBs that GRB 050709 and GRB 050724 exhibited long-lasting X-ray flares that occurred at least 100 s after triggering the bursts. While the observations have been claimed to be suggestive for compact mergers, it is not immediately clear whether the merger model can accommodate this late time X-ray flaring activity. The standard central engine, black hole plus disk, has –at least in its most simple form– difficulties to accommodate these long time scales. The dynamical timescale for an accretion disk is

$$\tau_{\rm d} \sim \frac{1}{\alpha \Omega_K} \sim 0.05{\rm s} \left(\frac{R}{200\ {\rm km}} \right)^{\frac{3}{2}} \left(\frac{0.1}{\alpha} \right) \left(\frac{2.5 M_\odot}{M_{\rm bh}} \right) \quad (11)$$

where α is the Shakura-Sunyaev viscosity parameter (Shakura & Sunyaev 1973) and Ω_K the angular frequency of a ring of matter at distance R. Obviously, the estimated accretion timescale is much shorter than the timescales at which the X-ray flaring activity is observed.

The X-ray activity might be caused by either a long-lived central engine, or by a wide distribution of Lorentz factors, or else by the deceleration of a Poynting flux dominated flow. Various possibilities are discussed in detail in Zhang et al. (2006). Here we want to address two possibilities: i) that the central object from a DNS merger survives for long enough to produce the flaring and ii) we also address the fallback accretion luminosity in the aftermath of a compact binary merger.

7.1. *Survival of the central object in a double neutron star merger*

The continued central engine activity could be due to the survival of the central object, either in a meta-stable state or –as discussed above– the remnant may in some cases loose enough mass to produce a stable, highly magnetised neutron star.

A meta-stable state is likely to occur, stabilisation could come for example from differential rotation (e.g. Morrison, Baumgarte, & Shapiro 2004) or trapped neutrinos together with non-leptonic negative charges (Prakash et al. 1995), but the time scale until collapse is uncertain. This is because all the imprecisely known aspects of the problem such as the EOS at supra-nuclear densities, the remnant radius and magnetic field, ellipticity of the central object and so on, enter with large powers in the estimate of the time scale. Therefore in the meta-stable case a large range of time scales until collapse can be expected for different initial binary systems. With reasonable parameters even time scales as long as weeks are possible (see Rosswog & Ramirez-Ruiz 2002b).

If the GRB is indeed caused by the combined action of neutrino annihilation and buoyant pockets of ultra-strong magnetic fields, this will plausibly also cause late-time flaring activity, provided that the remnant is stable for long enough. The magnetic field amplification acts on a time scale of about a milli-second (Price & Rosswog 2006) and thus large magnetic fields can be built up before the neutrino luminosity has reached its peak at $\approx$ 20 ms after the merger, see Figure 13. In the early stages a buoyant high-field bubble can expand into a practically baryon-free environment and thus reach large Lorentz-factors. At neutrino luminosities in excess of 10^{52} erg/s the remnant also drives a very energetic baryonic wind. If the right conditions are met, the baryonic material can help to collimate the outflow (Aloy et al. 2005), but it also poses a potential threat to the emergence of an ultra-relativistic outflow. Initially, as the rapidly spinning remnant produces high-field pockets in rapid succession, magnetic pressure may help to keep the funnel above the central object baryon-clean. But as the remnant is constantly braked by magnetic fields and gravitational wave emission, it takes longer and longer to reach buoyancy field strength, while more and more baryons are ablated from the remnant by neutrinos. The first explosive reconnection events escape into a very clean environment, those produced later will

be released into an envelope of neutrino-magneto-centrifugally expelled baryons. This different baryon loading may be responsible for the difference between bursts and X-ray flares.

7.2. *Fallback accretion*

Some of the matter expelled by gravitational torques is still gravitationally bound to the central object, and will fall back towards the remnant (see for example Figure 2, panel three). Direct numerical calculations over the interesting timescales are not feasible, therefore we follow a simplified analytical approach. We assume that the motion of this material can be approximated as Keplerian motion in a central potential produced by the remnant. From the total energy, E_i, and the angular momentum, J_i, of each SPH-particle the eccentricity of the particle orbit, e_i, can be calculated

$$e_i^2 = 1 + \frac{2E_i J_i^2}{G^2 m_i^3 M^2}. \qquad (12)$$

Here, m_i is the particle and M the enclosed mass. For the particles with $e_i < 1$, the semi-major axes are calculated, $a_i = -Gm_iM/(2E_i)$, from which the distances of the closest and farthest approach follow: $R_{\rm min} = a_i(1-\epsilon_i)$ and $R_{\rm max} = a_i(1+\epsilon_i)$. A particle with a velocity $\vec{v}_i$ that is currently located at radius r_i will reach the radius $R_{\rm dis}$ after a time of

$$\tau_i = \begin{cases} I_{r_i,r_{{\rm max},i}} + I_{r_{{\rm max},i},R_{\rm dis}} & \text{for} \quad \vec{v}_i \cdot \vec{r}_i > 0 \\ I_{r_i,R_{\rm dis}} & \text{for} \quad \vec{v}_i \cdot \vec{r}_i < 0 \end{cases}, \qquad (13)$$

where I_{r_1,r_2} is given by

$$I_{r_1,r_2} = \left[\frac{\sqrt{Ar^2+Br+C}}{A} + \frac{B}{2A\sqrt{-A}} \arcsin\left(\frac{2Ar+B}{\sqrt{-D}} \right) \right]_{r_1}^{r_2} \qquad (14)$$

with $D = 4AC - B^2$ and $A = \frac{2E_i}{m_i}$, $B = 2GM$ and $C = -\frac{J_i^2}{m_i^2}$ (Rosswog 2006).

For the radius, where the fallback energy is dissipated, $R_{\rm dis}$, we take in the double neutron star case the disk radius at the end of the numerical simulation. This is conservative in the sense that the disk will shrink, see below, and therefore the assumption of a radius fixed at $R_{\rm dis}$ yields shorter timescales and lower accretion luminosities. For the black hole cases, I choose $R_{\rm dis} = 10GM/c^2$, so just outside the innermost stable circular orbit of a non-rotating (Schwarzschild-) black hole at $R_{\rm ISCO} = 6GM/c^2$.

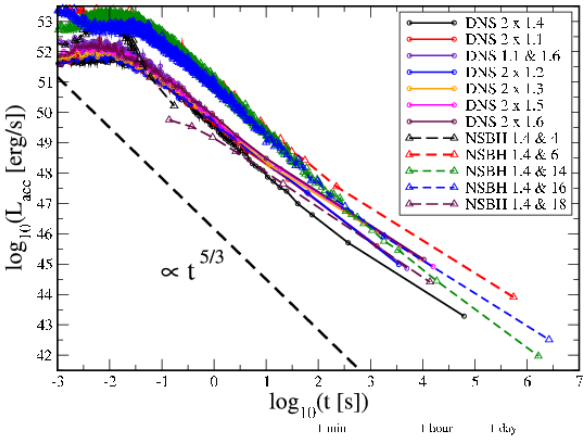

Fig. 18. Fallback accretion luminosity for various compact binaries, taken from Rosswog (2006). Circles refer to double neutron star systems (DNS), triangles to neutron star black hole mergers (NSBH). Note that the rightmost point is determined by the mass resolution of the simulation. For reference a straight line with slope 5/3 is shown.

The details of the fallback times and energies change slightly with $R_{\rm dis}$, but none of the conclusions depends on the exact numerical value of $R_{\rm dis}$.

Figure 18 shows the accretion luminosities, $L_{\rm acc} = dE_{\rm fb}/dt$, derived for various DNS and NSBH systems, for details see Rosswog (2006). Here, $E_{\rm fb}$ denotes the difference between the potential plus kinetic energy at the start radius, r_i, and the potential energy at the dissipation radius, $R_{\rm dis}$. The curves have been obtained by binning the energies contained in the fallback material, $E_{\rm fb}$, according to the corresponding fallback times, τ_i, see Equation (13). A fraction ϵ of this energy is channeled into X-rays, $L_X = \epsilon L_{\rm acc}$.

The double neutron star cases are rather homogeneous with respect to their fallback accretion, in all cases the fallback material is approximately 0.03 $M_\odot$[4]. After an initial, short-lived plateau the luminosity falls off with time close to the expected 5/3-power law(Rees 1988; Phinney 1989). The last point in these curves is determined by the numerical mass resolution in the hydrodynamics simulations and should therefore be interpreted with some caution. All other points should be a fair representation of the overall fallback activity. Typically, the X-ray luminosity about one hour after the coalescence is $L_X \sim \left(\frac{\epsilon}{0.1}\right) \cdot 10^{44}$ erg/s. For the investigated mass

[4]General relativistic effects might reduce this number somewhat.

range the spread in the luminosities one hour after the coalescence is about one order of magnitude.

The neutron star black hole cases show a larger diversity. The mass in the fallback material of different mass ratios varies by about a factor of 500, see Rosswog (2006), an hour after the merger the accretion luminosities of the different NSBH systems differ by about two orders of magnitude. The involved time scales change strongly with the binary mass ratio. For example, the 1.4 and 4 $M_\odot$ NSBH case does not produce much eccentric fallback material. Accretion, at least to the resolvable level, is over in ~ 0.2 s. This accretion period may produce a short GRB, but probably not much X-ray activity. The 1.4 and 18 $M_\odot$ NSBH system is at the other extreme: its peak luminosity is lower by three orders orders of magnitude but extends (at a resolvable level) up to about one hour. The mass ratios in-between could possibly produce a (weak) GRB and extended X-ray activity up to about one day after the burst.

8. SUMMARY

We have discussed various aspects of the last stages in the life of a compact binary. In particular we have addressed

- Gravitational waves as a probe of the merger dynamics

  We have shown how the merger dynamics is imprinted on the gravitational wave signal. Examples include the peak gravitational wave frequency of a double neutron star merger and the subsequent ringdown emission which both are sensitive to the equation of state. For a stiff EOS, low-mass black hole neutron star systems undergo a long-lived, mostly episodic mass transfer phase. We show an example where the mass transfer continues for as long as 47 orbital periods. This last binary phase is responsible for a gravitational wave signal with slowly decaying amplitude and increasing frequency. The signal only shuts off when the neutron star is finally disrupted upon reaching its minimum mass. The coincident of detection of a short GRB together with a "chirping" gravitational wave signal would be the ultimate proof of a compact binary central engine.

- Accretion disks

  Compact binary mergers produce in some (but not all) cases accretion disks from the neutron star debris. These disks differ from the standard thin disk accretion model in various ways. Due to insufficient cooling by neutrinos they are often thick and puffed up, they are usually neither in a dynamical nor in β-equilibrium. For double neutron star mergers they are generally massive, of order 0.25 $M_\odot$, with temperatures of several MeV and an electron fraction of close to 0.1 (at least initially). For neutron star black hole systems we find it substantially more difficult to form massive disks. For low-mass black hole systems, the initial episodic mass transfer with a surviving neutron star prevents the build up of a massive disk. Only after a complete disruption of the neutron star a disk of ≈ 0.05 $M_\odot$ forms. A comparison of the debris masses in double neutron star and neutron star black hole mergers is shown in Figure 11. We find the neutron star black hole systems to produce disks masses that are lower by at least a factor six. For higher mass black holes the neutron star is disrupted early on, but very close to the innermost stable circular orbit. The resulting accretion disks are geometrically thin and essentially cold. For black hole masses larger that about 16 $M_\odot$ no disk forms at all, most of the neutron star is fed directly into the hole, the rest is dynamically ejected. These results are sensitive to the equation of state, for a softer equation of state the neutron star is disrupted more easily.

- Gamma-ray bursts

  Neutrino annihilation from the remnant of a double neutron star merger can plausibly provide the driving stresses to launch highly relativistic, bipolar outflows, but a large diversity in the observable burst properties and moderate burst energies of $\sim 10^{48}$ are expected. It is conceivable that a good fraction of systems fails to provide the right conditions and instead produces X-ray or UV-flashes. MHD simulations of double neutron star mergers show that the magnetic field grows within the first millisecond to (probably much) beyond magnetar strength, possibly allowing for a burst production à la Kluzńiak & Ruderman (1998). The burst is most likely a result of the combined action of both neutrino annihilation and ultrastrong magnetic field. Of the neutron star black hole binaries only systems with low black hole masses could possibly form disks that are hot and dense enough to launch GRBs (unless the true nuclear equation of state is much softer than the one we use here). Among them, rapidly spinning holes are preferred as both the last sta-

ble orbit and the event horizon move closer to the hole. The high-mass end of neutron star black hole binaries probably produces a low-luminosity tail of the short GRB-distribution.

- Magnetar formation

  If the maximum neutron star mass should indeed be as high as indicated by recent observations the amount of mass that would need to be lost after a merger to evade the final collapse to a black hole is not implausibly large. Therefore we want to point out the possibility that binary systems from the lower end of the mass distribution could produce a highly magnetised, but stable neutron star rather than a black hole. Magnetars outside normal supernova remnants would be obvious candidates for this formation channel. If true, this channel should also produce large amounts of neutron-rich nuclei synthesised in both the dynamically ejected neutron star material and in the neutrino-magnetocentrifugal wind that made the survival of the remnant possible in the first place. Being synthesised in a neutrino bath dominated by electron anti-neutrinos the wind material will to be more proton-rich than the dynamically ejected material. The exact Y_e is determined by both the expansion time scale and the ratio of neutrino and anti-neutrino luminosities, but is roughly (Qian & Woosley 1996)

$$Y_e \sim 0.28 \left[1 + \frac{L_{\bar{\nu}_e}/5 \cdot 10^{52}\mathrm{erg}}{L_{\nu_e}/2 \cdot 10^{52}\mathrm{erg}}\right]^{-1}, \qquad (15)$$

  where L_{ν_e} and $L_{\bar{\nu}_e}$ are the electron neutrino and anti-neutrino luminosities, respectively. The more neutron-rich dynamical ejecta with $Y_e \approx 0.1$ would be expected to be located at larger distances from the magnetar than the wind material.

- Late time X-ray activity

  In the speculative case that the central object of a neutron star merger survives, late-time flaring would be caused by the same mechanism that produced the burst. If the burst is (at least in part) produced by explosive reconnection events of buoyant high-field bubbles as suggested by Kluzńiak & Ruderman (1998), parts of the remnant that become buoyant at later times have to expand into an environment that is already heavily baryon-polluted by neutrino-driven winds. Due to the higher baryon loading the emission would be mainly in the X-ray band of the spectrum.

  Much less speculative is the accretion of fall-back material which occurs naturally in the aftermath of a compact binary merger. A few percent of a solar mass are ejected into eccentric, but still bound orbits. The fallback of this material produces extended X-ray activity up to many hours after the main burst.

Some of the figures have been produced using the software SPLASH kindly provided by Daniel Price. The calculations shown in this paper were in part performed on the JUMP system of the Höchstleistungsrechenzentrum Jülich. It is a pleasure to thank Joe Monaghan and Andrew Melatos for their hospitality during the last stages of writing this paper.

REFERENCES

Abramovici, A., et al. 1992, Science, 256, 325 (http://www.ligo.caltech.edu)
Akmal, A., Pandharipande, V. R., & Ravenhall, D. G. 1998, Phys. Rev. C, 58, 1804
Aloy, M. A., Janka, H.-T., & Müller, E. 2005, A&A, 436, 273
Ando, M., et al. 2004, Class. Quant. Grav., 21, 1679
Asano, K., & Fukuyama, T. 2001, ApJ, 546, 1019
Ayal, S., et al. 2001, ApJ, 550, 846
Balbus, S. A., & Hawley, J. F. 1998, Rev. Mod. Phys., 70, 1
Barthelmy, S., et al. 2005, Nature, 438, 994
Baumgarte, T., & Shapiro, S. L. 2003, Phys. Rep., 376, 41
Berger, E., et al. 2005, Nature, 438, 988
Berger, E., et al. 2006a, astro-ph/0602004
Berger, E., et al. 2006b, ApJ, submitted (astro-ph/0611128)
Blanchet, L. 2006, Living Rev. Rel., 9, 4
Blandford, R. D., & Znajek, R. L, 1977, MNRAS, 179, 433
Blandford, R. D., & Payne, D. G., 1982, MNRAS, 199, 883
Blinnikov, S., et al. 1984, Soviet Astron. Lett., 10, 177
Bloom, J., et al. 1999, Nature, 401, 453
Bloom, J., et al. 2006, ApJ, 638, 354
Burgay, M., et al. 2003, Nature, 426, 4
Chandrasekhar, S. 1975, ApJ, 202, 809
Chen, W.-X., & Beloborodov, A. M. 2006, ApJ, accepted (astro-ph/0607145)
Chow, E., & Monaghan, J. J., 1997, J. Comp. Phys., 134, 296
Cook, G. B., Shapiro, S. L., & Teukolsky, S. A. 1996, Phys. Rev. D, 53, 5533

Costa, E., et al. 1997, Nature, 387, 783
Cutler, C., & Flanagan, É. E. 1994, Phys. Rev. D, 49, 2658
DiMatteo, T., et al. 2002, ApJ, 579, 706
Duncan, R. C., & Thompson, C. 1992, ApJ, 392, L9
Eichler, D., et al. 1989, Nature, 340, 126
Faber, J. A., & Rasio, F. A. 2000, Phys. Rev. D, 62, 064012
Faber, J., et al. 2002, Phys. Rev. Lett., 89, 231102
Faber, J., et al. 2004, Phys. Rev. D, 69, 124036
Faber, J., et al. 2006, Phys. Rev. D, 73, 024012
Faulkner, A. J., et al. 2005, ApJ, 618, L119
Ferrario, L., & Wickramasinghe, D. T. 2005, MNRAS, 356, 615
Fox, D. B., et al. 2005, Nature, 437, 845
Frail, D., et al. 1997, Nature, 389, 261
Freise, A. 2005, Class. Quant. Grav., 22, S869
Fryer, C., & Kalogera, V. 2001, ApJ, 554, 548
Grote, H., et al. 2005, Class. Quant. Grav., 22, 193
Hjorth, J., et al. 2003, Nature, 423, 857
Hjorth, J., et al. 2005, Nature, 437, 859
Isenberg, J. A. 1978, preprint
Janka, H.-T., Eberl, T., Ruffert, M., & Fryer, C. L. 1999, ApJ, 527, L39
Kalogera, V., et al. 2004, ApJ, 614, L137
Kippenhahn, R., & Weigert, A. 1990, Stellar Structure and Evolution (Berlin: Springer)
Kluźniak, W., & Ruderman, M. 1998, ApJ, 505, L113
Kobayashi, S., & Mészáros, P. 2003, ApJ, 589, 861
Kohri, K., & Mineshige, S. 2002, ApJ, 577, 311
Kouveliotou, C., et al. 1993, ApJ, 413, L101
Lai, D., et al. 1993, ApJS, 88, 205
Lattimer J. M., & Swesty, F. D. 1991, Nucl. Phys., A535, 331
Lee, W. H., & Kluźniak, W. L. 1999a, MNRAS, 308, 780
Lee, W. H., & Kluźniak, W. L. 1999b, ApJ, 526, 178
Lee, W. H. 2000, MNRAS, 318, 606
Lee, W. H. 2001, MNRAS, 328, 583
Lee, W. H., & Ramirez-Ruiz, E. 2002, ApJ, 577, 893
Lee, W. H., et al. 2005, ApJ, 632, 421
Löffler, F., Rezzolla, L., & Ansorg, M. 2006, gr-qc/0606104
Lyutikov, M., et al. 2003, ApJ, 597, 998
MacFadyen, A. I., Ramirez-Ruiz, E., & Zhang, W. 2005, astro-ph/0510192
McKinney, J. C. 2005, astro-ph/0506369
Mészáros, P., & Rees, M. J. 1997, ApJ, 482, L29
Mészáros, P. 2006, Rep. Prog. Phys., 69, 2259
Mochkovitch, R., et al. 1993, Nature, 361, 236
Monaghan, J. J. 2002, MNRAS, 335, 843
Morrison, I., Baumgarte, T., & Shapiro, S. L. 2004, ApJ, 610, 941
Nakar, E., Gal-Yam, A., & Fox, D. B. 2006, ApJ, 650, 281
Narayan, R., Piran, T., & Shemi, A. 1991, ApJ, 379, L17
Narayan, R., Piran, T., & Kumar, P. 2001, ApJ, 557, 949
Nice, D., et al. 2005, ApJ, 634, 1242
Oechslin, R., et al. 2002, Phys. Rev. D, 65, 103005
Oechslin, R., et al. 2004, MNRAS, 349, 1469
Oechslin, R., Janka, H.-T., & Marek, A. 2006, A&A, submitted (astro-ph/0611047)
Özel, F. 2006, Nature, 441, 1115
Oohara, K., & Nakamura, T. 1989, Prog. Theor. Phys., 82, 535
van Paradijs, J., et al. 1997, Nature, 386, 686
Paczyński, B., & Wiita, P. J. 1980, A&A, 88, 23
Paczyński, B. 1991, Acta Astronomica, 41, 257
Phinney, E. S. 1989, in IAU Symp. 136, The Center of the Galaxy, ed. M. Morris (Dordrecht: Kluwer), 543
Piran, T. 2005, Rev. Mod. Phys., 76, 1143
Popham, R. C., et al. 1999, ApJ, 518, 356
Prakash, M., et al. 1995, Phys. Rev. D, 52, 661
Price, D. J. 2004, PhD Thesis, University of Cambridge, UK
Price, D. J., & Monaghan, J. J. 2005, MNRAS, 364, 384
Price, D. J., & Monaghan, J.J. 2007, MNRAS, 374, 1347
Price, D. J., & Rosswog, S. 2006, Science, 312, 719
Psaltis, D. 2006, in Compact Stellar X-ray Sources, ed. W. H. G. Lewin & M. van der Klis (Cambridge: Cambridge University Press)
Qian, Y.-Z., & Woosley, S. E. 1996, ApJ, 471, 331
Rasio, F., & Shapiro, S. A. 1994, ApJ, 432, 242
Rees, M. J. 1988, Nature, 333, 523
Rhoades, C. E., & Ruffini, R. 1974, Phys. Rev. Lett., 32, 324
Rosswog, S., et al. 2000, A&A, 360, 171
Rosswog, S., & Davies, M. B. 2002a, MNRAS, 334, 481
Rosswog, S., & Ramirez-Ruiz, E. 2002b, MNRAS, 336, L7
Rosswog, S., & Liebendörfer, M. 2003a, MNRAS, 342, 673
Rosswog, S., & Ramirez-Ruiz, E. 2003b, MNRAS, 343, L36
Rosswog, S., Ramirez-Ruiz, E., & Davies, M. B. 2003c, MNRAS, 345, 1077
Rosswog, S., et al. 2004, MNRAS, 351, 1121
Rosswog, S. 2005, ApJ, 634, 1202
Rosswog, S. 2006, MNRAS, in press (astro-ph/0611440)
Rosswog, S., & Price, D. J., 2006, in preparation
Ruffert, M., et al. 1997, A&A, 319, 122
Ruffert, M., & Janka, H. T. 2001, A&A, 380, 544
Sasaki, M., et al. 2004, ApJ, 617, 322
Setiawan, S., Ruffert, M., & Janka, H.-T. 2004, MNRAS, 352, 753
_____. 2006, A&A, 458, 553
Shakura, N. I., & Sunyaev, R. A. 1973, A&A, 24, 337
Shen, H., et al. 1998, Prog. Theor. Phys., 100, 1013
Shibata, M. 1999, Phys. Rev. D, 60, 104052
Shibata, M., & Uryu, K. 2002, Prog. Theor. Phys., 107, 265
Shibata, M., et al. 2005, Phys. Rev. D, 71, 4021
Shibata, M., & Uryu, K. 2006, astro-ph/0611522

Spallicci, A., et al. 2005, Class. Quant. Grav., 22, 461
Springel, V., & Hernquist, L. 2002, MNRAS, 333, 649
Stairs, I. 2004, Science, 304, 547
Stanek, K. Z., et al. 2003, ApJ, 591, L17
Stern, D. 1970, Am. J. Phys., 38, 494
Taniguchi, K., et al. 2005, Phys. Rev. D, 72, 044008
Tassoul, M. 1975, ApJ, 202, 803
Thompson, C. 1994, MNRAS, 270, 480
Thompson, C., & Duncan, R. 1993, ApJ, 408, 194
_____. 1995, MNRAS, 275, 255
Thompson, T. A., Burrows, A., & Meyer, B. S. 2001, ApJ, 562, 887
Thompson, T. A., Chang, P., & Quataert, E. 2004, ApJ, 611, 380
Thorsett, S. E., & Chakrabarty, D. 1999, ApJ, 512, 288
Usov, V. V. 1992, Nature, 357, 472
Vink, J. 2006, in IAU Symp. 230, Populations of High Energy Sources in Galaxies, ed. E. J. A. Meurs & G. Fabbiano (Cambridge: Cambridge University Press), 16
Villasenor, J. S., et al. 2005, Nature, 437, 855
Will, C. M. 2005, Phys. Rev. D, 71, 084027
Wilson, J. R., et al. 1996, Phys. Rev. D, 54, 1317
Zhang, B., et al. 2006, ApJ, 642, 354

Stephan Rosswog: School of Engineering and Science, International University Bremen, Campus Ring 1, D-28759 Bremen, Germany (s.rosswog@iu-bremen.de).